bioRxiv preprint doi: https://doi.org/10.1101/123547; this version posted April 3, 2017. The copyright holder for this preprint (which was not certified by peer review) is the author/funder, who has granted bioRxiv a license to display the preprint in perpetuity. It is made available under aCC-BY-NC-ND 4.0 International license.

Giantin knockout models reveal the capacity of the Golgi to regulate its biochemistry by controlling glycosyltransferase expression

Nicola L. Stevenson[1], Dylan J. M. Bergen[1], Roderick E.H. Skinner[2], Kate A. Robson Brown[3], Chrissy L. Hammond[2], and David J. Stephens[1]

[1] Cell Biology Laboratories, School of Biochemistry, University of Bristol, Biomedical Sciences Building, University Walk, Bristol, UK, BS8 1TD;

[2] School of Physiology, Pharmacology and Neuroscience, University of Bristol, Biomedical Sciences Building, University Walk, Bristol, UK, BS8 1TD;

[3] Computed Tomography Laboratory, School of Arts, University of Bristol, 43 Woodland Road, Bristol BS8 1UU

* Corresponding author and lead contact: david.stephens@bristol.ac.uk

Number of characters: 48,150

bioRxiv preprint doi: https://doi.org/10.1101/123547; this version posted April 3, 2017. The copyright holder for this preprint (which was not certified by peer review) is the author/funder, who has granted bioRxiv a license to display the preprint in perpetuity. It is made available under aCC-BY-NC-ND 4.0 International license.

Summary

The Golgi is the cellular hub for glycosylation, controlling accurate processing of complex proteoglycans and glycolipids. Its structure and organisation is dependent on golgins which tether cisternal membranes and incoming transport vesicles. Here we show that knockout of the largest golgin, giantin, leads to substantial changes in gene expression despite only limited effects on Golgi structure. Notably, 22 Golgi-resident glycosyltransferases, but not glycan processing enzymes or the ER glycosylation machinery, are differentially expressed following giantin ablation. Most of these glycosyltransferases are highly downregulated following genetic knockout of giantin, including a near-complete loss of expression of GALNT3 in both mammalian cell and zebrafish models. Furthermore, knockout zebrafish exhibit increased bone mass density, hyperostosis, and ectopic calcium deposits recapitulating phenotypes of hyperphosphatemic familial tumoral calcinosis, a disease caused by mutations in GALNT3. Our data reveal a new feature of Golgi homeostasis, the ability to regulate glycosyltransferase expression to generate a functional proteoglycome.

Keywords

Golgi, giantin, glycosylation, GALNT3, hyperphosphatemic tumoral calcinosis, zebrafish.

bioRxiv preprint doi: https://doi.org/10.1101/123547; this version posted April 3, 2017. The copyright holder for this preprint (which was not certified by peer review) is the author/funder, who has granted bioRxiv a license to display the preprint in perpetuity. It is made available under aCC-BY-NC-ND 4.0 International license.

Introduction

Golgins are coiled-coil domain proteins that project out from the surface of the Golgi apparatus into the cytosol (Gillingham and Munro, 2016). They maintain Golgi organisation and selectively tether incoming transport vesicles seeking to fuse with Golgi cisternae. The largest golgin family member is giantin, whose N-terminal cytosolic domain has a predicted molecular mass of 370kDa (Linstedt and Hauri, 1993). Giantin is one of only three golgins to have a C-terminal transmembrane domain, directly anchoring it within cis- and medial-Golgi membranes.

The functional role of giantin is poorly defined. Early *in vitro* studies suggest that giantin resides in COPI vesicles; transport carriers mediating intra-Golgi and retrograde Golgi-to-endoplasmic reticulum (ER) transport (Sönnichsen et al., 1998). Here giantin is reported to recruit p115, which binds simultaneously to GM130 on cis-Golgi membranes to mediate tethering. Giantin-p115 interactions may also facilitate GM130-independent retrograde transport (Alvarez et al., 2001). In addition to p115, giantin has been shown to interact with GCP60 (Sohda et al., 2001), Rab1 and Rab6 (Rosing et al., 2007). Rab1 and Rab6 localise to ER-Golgi- and retrograde transport vesicles respectively and thus their interaction with Golgi-resident giantin could similarly promote vesicle capture. Giantin is also implicated in lateral Golgi tethering (Koreishi et al., 2013) and ciliogenesis (Asante et al., 2013).

Giantin knockout (KO) rodent models vary in phenotype. Homozygous knockout rats, possessing a null mutation in the *Golgb1* gene encoding giantin, develop osteochondrodysplasia (Bergen et al., 2017; Katayama et al., 2011). Embryonic phenotypes include systemic oedema, cleft palate, craniofacial defects and shortened long bones and are largely attributed to defects in chondrogenesis. Interestingly, cells from mutant animals have expanded ER and Golgi membranes whilst growth plates contain less extracellular matrix (ECM), indicative of secretory pathway defects (Katayama et al., 2011). Mouse giantin KO models have less complex developmental disorders, the most predominant phenotype being

bioRxiv preprint doi: https://doi.org/10.1101/123547; this version posted April 3, 2017. The copyright holder for this preprint (which was not certified by peer review) is the author/funder, who has granted bioRxiv a license to display the preprint in perpetuity. It is made available under aCC-BY-NC-ND 4.0 International license.

cleft palate (Lan et al., 2016). These animals also have ECM abnormalities associated with glycosylation defects but Golgi structure is normal in this instance (Lan et al., 2016). Work from our lab has also now characterised giantin function in zebrafish (Bergen et al., 2017). In contrast to rodent models, homozygous giantin KO zebrafish do not show any gross morphological changes during development, can reach adulthood, and show only a minor growth delay. They do however show defects in cilia formation and length consistent with our previous work *in vitro* (Asante et al., 2013).

There are two major pathways of protein glycosylation, *N*- and *O*-glycosylation initiated in the ER and Golgi respectively. Most oligosaccharides are then subject to modification and extension by Golgi-resident type II transmembrane glycosyltransferases, the importance of which is underscored by the clear link between Golgi dysfunction and congenital disorders of glycosylation (Freeze and Ng, 2011). Mucin-type O-glycosylation is the most prevalent form of glycosylation on cell surface and secreted proteins. It is initiated by Golgi-resident polypeptide *N*-acetylgalactosaminyltransferases (GALNTs) that catalyse the addition of *N*-acetylgalactosamine to serine or threonine residues on target substrates (forming the Tn antigen, (Bennett et al., 2012)). There are twenty GALNT proteins in humans with distinct but overlapping substrate specificities and spatio-temporal expression patterns (Bard and Chia, 2016; Schjoldager et al., 2015). Such redundancy means mutations in GALNT genes produce very mild phenotypes. Several genome-wide association studies have linked GALNTs with diverse pathologies such as Alzheimer's disease (Beecham et al., 2014) and obesity (Ng et al., 2012). Mutations in GALNT3 have been linked directly to human disease (Ichikawa et al., 2007; Topaz et al., 2004). Complete loss of GALNT3 function results in a failure to *O*-glycosylate FGF23, leading to its inactivation and the subsequent development of hyperphosphatemic familial tumoral calcinosis (HFTC, (Kato et al., 2006)). HFTC is characterised by hyperostosis and the ectopic deposition of calcium in skin and subcutaneous tissues.

bioRxiv preprint doi: https://doi.org/10.1101/123547; this version posted April 3, 2017. The copyright holder for this preprint (which was not certified by peer review) is the author/funder, who has granted bioRxiv a license to display the preprint in perpetuity. It is made available under aCC-BY-NC-ND 4.0 International license.

99 In the absence of a clearly defined role for giantin at the Golgi, we sought to study its function in an

100 engineered KO cell line. In this system, as well as a zebrafish model, we show for the first time that

101 giantin regulates the expression of Golgi-resident glycosyltransferases.

102

bioRxiv preprint doi: https://doi.org/10.1101/123547; this version posted April 3, 2017. The copyright holder for this preprint (which was not certified by peer review) is the author/funder, who has granted bioRxiv a license to display the preprint in perpetuity. It is made available under aCC-BY-NC-ND 4.0 International license.

Results

Generation of a giantin KO cell line

We generated a KO cell line for GOLGB1 (giantin) using genome editing. A GFP-fusion of the double nickase mutant of Cas9 (Cas9D10A-GFP) was co-transfected into human non-transformed telomerase immortalized retinal pigment epithelial (hTERT-RPE1) cells with paired guide RNAs targeting exon 7 of the *GOLGB1* gene. GFP-positive cells were then sorted by FACS, screened for loss of giantin by immunofluorescence, and sequenced at the target site. Using this approach, one clone was identified with an indel frameshift mutation in both alleles, leading to a frameshift and premature stop codon (R195fsX204-R195P-A196del, Figure 1A). The full length giantin coding sequence is 3269 amino acids. Downstream of the mutation an in-frame translational start site was also noted with the potential to permit expression of a truncated protein. To exclude this possibility, we probed the mutant cells for giantin expression using three different antibodies raised against the full length, C-, and N-termini of the protein. No protein was detected by immunoblot or immunofluorescence (Figure 1B-D).

Loss of giantin does not lead to gross defects in Golgi morphology or trafficking

As giantin resides at the Golgi apparatus, we began characterizing the KO cell line by examining Golgi morphology. KO cells were immuno-labelled for Golgi markers and the size and number of Golgi elements quantified. No significant change in Golgi structure was detected (Figure 2A-C). The relative distribution of *cis*- and *trans*-Golgi markers was also maintained, suggesting organelle polarity was unperturbed (Figure 2D). Similarly, the general organisation of the early secretory pathway was normal (Figure 2E, showing labelling for ER exit sites and ER-Golgi intermediate compartment). We therefore decided to study Golgi morphology in greater detail by electron microscopy (EM). At this resolution, Golgi stacks had comparable numbers of cisternae in WT and KO cells and cisternae were of equivalent

bioRxiv preprint doi: https://doi.org/10.1101/123547; this version posted April 3, 2017. The copyright holder for this preprint (which was not certified by peer review) is the author/funder, who has granted bioRxiv a license to display the preprint in perpetuity. It is made available under aCC-BY-NC-ND 4.0 International license.

length with no sign of dilation (Figure 2F-H). Overall these results suggest Golgi structure was not grossly disrupted following loss of giantin.

Many golgins have been shown to act as tethers for transport vesicles but such a function has not yet been defined for giantin (Wong and Munro, 2014). To test whether giantin is involved in trafficking, we used the Retention Using Selective Hooks (RUSH) system (Boncompain et al., 2012) to monitor ER-to-Golgi transport. In this assay a fluorescently-labelled Golgi-resident protein (the reporter, here EGFP-tagged mannosidase I) is fused to streptavidin binding protein (SBP) and co-expressed with an ER-resident protein fused to streptavidin (the hook, here tagged with a KDEL motif). When both engineered fusion proteins are present, the SBP on the reporter binds to the streptavidin on the hook and is retained in the ER. Reporter release is then induced by the addition of biotin, which outcompetes the SBP for streptavidin binding. Time-lapse imaging of biotin treated KO cells expressing this RUSH construct (Supplemental Movies S1 and S2) showed a slight delay and greater variability in anterograde mannosidase I trafficking relative to WT, however this difference was not statistically significant (Figure 2I-J). In order to analyse a greater number of cells, we repeated this experiment but fixed cells at 0, 10 and 20 minutes post-biotin addition and quantified cargo delivery at each time point. This approach also allowed us to confirm that we were observing ER-Golgi transport as we could co-label the Golgi (Figure 2L). Again, giantin KO cells showed no significant delay in anterograde transport compared to WT cells (Figure 2K-L).

Perturbations in anterograde trafficking can result in ER stress and activation of the unfolded protein response (UPR) as secretory cargo accumulates in this compartment (Brodsky, 2012). We found that expression of classical markers of the UPR including PERK, calnexin and CHOP was unchanged in giantin KO cells compared to controls (Figure 2M) suggesting no activation of the UPR in giantin KO cells.

GM130 localisation is altered in giantin KO cells following Golgi fragmentation

bioRxiv preprint doi: https://doi.org/10.1101/123547; this version posted April 3, 2017. The copyright holder for this preprint (which was not certified by peer review) is the author/funder, who has granted bioRxiv a license to display the preprint in perpetuity. It is made available under aCC-BY-NC-ND 4.0 International license.

148 During mitosis, the Golgi must disassemble and reassemble. As we could not detect any gross defects in
149 Golgi structure in giantin KO cells at steady state, we analysed Golgi dynamics by chemically inducing its
150 disassembly. First, we treated cells with nocodazole, which disassembles microtubules and thus causes
151 Golgi ribbons to fragment into polarised mini-stacks (Thyberg and Moskalewski, 1985). Under these
152 conditions, the dynamics of disassembly and reassembly were found to be equivalent in both cell lines
153 (Figure 3A), with fragmentation of the TGN preceding that of the cis-Golgi as reported previously (Yang
154 and Storrie, 1998). Likewise, Golgi disassembly following brefeldin A treatment (which inhibits the Arf-
155 guanine nucleotide exchange factor, GBF1) was comparable in WT and KO cells (Figure S1). We also
156 failed to find any defects in cell cycle progression using propidium iodide labelling and flow cytometry
157 (data not shown).

158 During these Golgi disruption experiments, we noticed a difference in GM130 labelling of WT and KO
159 cells. Following nocodazole treatment, giantin reportedly persists on the original fragmenting
160 membranes (the 'old Golgi') rather than cycling through the ER onto immature peripheral mini-stacks
161 (Fourriere et al., 2016; Nizak et al., 2003). This is apparent here in WT cells, which show an enrichment
162 of giantin on larger, juxtanuclear structures over more peripheral elements (Figure 3A). In KO cells,
163 however, these larger Golgi elements appear to be enriched with GM130. This enrichment is not due to
164 upregulation of GM130 expression as protein levels are equivalent in WT and KO cells (Figure 3B-C),
165 suggesting instead that GM130 has either redistributed between Golgi membranes, perhaps to
166 compensate for giantin, or is labelling larger structures not present in WT cells. To distinguish between
167 these possibilities, we examined cells treated with nocodazole for 90 minutes by EM. As expected larger,
168 perinuclear 'old Golgi' structures could be detected in both WT and KO cells, as well as peripheral mini-
169 stacks (Figure 3D). The size distribution of these structures was equivalent in both cell lines (Figure 3E-F).
170 The larger GM130-labelled elements must therefore reflect a redistribution of the protein.

171 *Giantin negative Golgi 'mini-stacks' show a tendency to circularize*

bioRxiv preprint doi: https://doi.org/10.1101/123547; this version posted April 3, 2017. The copyright holder for this preprint (which was not certified by peer review) is the author/funder, who has granted bioRxiv a license to display the preprint in perpetuity. It is made available under aCC-BY-NC-ND 4.0 International license.

Surprisingly, EM of nocodazole-treated KO cells showed Golgi elements that had apparently circularized (Figure 3D, insets). These were absent in WT and untreated KO cells, except for one case of the latter. To quantify curvature of fragmented Golgi elements we calculated the angle between two lines drawn from each Golgi rim to the centre of the stack; circularised Golgi structures were assigned an angle of 0^{o} and linear stacks 180^{o}. This analysis showed a significant overall trend towards horseshoe-shaped and circular stacks in the KO cells compared to the WT (Figure 3G). Giantin-deficient Golgi stacks therefore exhibit structural abnormalities with low frequency (5% of structures/at least one present in 14% of cells) once fragmented.

Glycosylation enzyme expression patterns are altered in giantin KO cells

Giantin is a highly-conserved gene essential for viability in rodents (Katayama et al., 2011; Lan et al., 2016) yet phenotypes in our KO cell line and indeed in KO zebrafish (Bergen et al., 2017) are mild. We therefore considered whether the cells had undergone adaptation, as has been reported for other KO systems (Rossi et al., 2015). Having established that the expression of other golgin family members was normal (Figure 3B-C), we performed RNAseq of WT and KO cells to compare gene expression patterns in an unbiased manner. Pairwise analysis of triplicate samples identified a total of 1519 genes showing a greater than 2-fold change in expression in KO cells. Of those, 807 genes exhibited a greater than 3-fold change in expression in KO cells (Supplementary Tables S1 & S2). Gene ontology analysis showed that major classes of genes that were differentially expressed encoded highly glycosylated proteins, extracellular matrix components, and adhesion proteins. Of note, twenty-four glycosyltransferases were differentially expressed between the two cell lines. These include a pseudogene (DPY19L2P2), an ER-resident glycosyltransferase (UGT8) and twenty-two type II Golgi-resident transmembrane enzymes (Table 1). Some of these were among the most highly downregulated genes overall. Notably, other ER-localized core glycosyltransferases, glycan processing and modifying enzymes, and the cytosolic glycosylation machinery were unchanged following KO of giantin.

bioRxiv preprint doi: https://doi.org/10.1101/123547; this version posted April 3, 2017. The copyright holder for this preprint (which was not certified by peer review) is the author/funder, who has granted bioRxiv a license to display the preprint in perpetuity. It is made available under aCC-BY-NC-ND 4.0 International license.

To determine the impact of altered glycosyltransferase expression in the KO cells, we looked at global glycosylation patterns using biotinylated lectins to label fixed cells. RCA_{120} labelling of β-D-galactosyl residues was more bundled in KO cells but otherwise there were no gross changes in glycan abundance or localisation (Figure S2). We also probed cell lysates with lectins by blotting and found only minor changes in glycosylation patterns, namely loss of a 25kDa band when labelling with either ConA or HABP which recognise α-D-mannosyl and α-D-glucosyl residues and hyaluronic acid respectively (Figure S2). Glycosylation patterns are therefore largely normal, but with some identifiable changes.

GALNT3 expression is dramatically reduced in giantin KO cells

To validate the findings of the RNAseq analysis, we first performed immunoblots for two of the more highly downregulated glycosyltransferases, GALNT3 and CHST11 for which reagents were available. This confirmed that expression of these enzymes was reduced at the protein level (Figure 4A-B). Immunolabelling of fixed cells further demonstrated a near-complete loss of GALNT3 expression in giantin KO cells (Figure 4C). *GALNT3* is mutated in the human disease HFTC (Topaz et al., 2004) and so we decided to focus our studies on this gene.

We hypothesised that downregulation of GALNT3 could have occurred in response to aberrant trafficking following the loss of giantin function; such mistargeting could result in degradation coupled with a feedback mechanism to downregulate expression. We tested this directly by expressing FLAG-tagged GALNT3 in WT and KO cells. Immunofluorescence labelling showed FLAG-GALNT3 is efficiently targeted to the Golgi in both cell lines (Figure 4D). GALNT3 localisation is thus independent of giantin function and not the cause of its down-regulation. We next decided to test whether GALNT3 down-regulation was reversible by reintroducing epitope-tagged giantin into KO cells. Giantin KO cells expressing flag-giantin for up to 2 weeks failed to show any recovery of GALNT3 protein expression (data not shown).

bioRxiv preprint doi: https://doi.org/10.1101/123547; this version posted April 3, 2017. The copyright holder for this preprint (which was not certified by peer review) is the author/funder, who has granted bioRxiv a license to display the preprint in perpetuity. It is made available under aCC-BY-NC-ND 4.0 International license.

Giantin KO zebrafish phenotypes are consistent with tumoral calcinosis

We next sought to explore the role of giantin in regulating glycosyltransferase expression *in vivo* using two recently characterised *golgb1* KO zebrafish lines (Bergen et al., 2017) carrying a point mutation (C>T) in exon 14 leading to generation of a premature stop codon at glutamine-2948 (denoted *golgb1*$^{Q2948X/Q2948X}$). The second allele was generated by TALEN mutagenesis introducing an 8bp insertion at exon 14. This results in a frameshift at position 3029 leading to a premature stop codon at position 3078 (E3027fsX3078-T3028_A3029del, denoted *golgb1*$^{3078X/3078X}$). Both mutations lead to loss of the transmembrane domain and therefore are expected to be loss-of-function mutations. These fish do not display any gross developmental defects but did have a mild developmental delay and defects in cilia function (Bergen et al., 2017).

First, we performed quantitative PCR of mixed bone and cartilage tissues from both mutant fish lines at 60 days post fertilization (dpf). In each case, we observed a significant loss of *galnt3* expression (Figure 5A) with one KO individual from each line possessing almost undetectable levels of transcript. Since the giantin KO fish reach adulthood and given the causative link between loss of GALNT3 and HFTC in humans, we next examined WT and mutant skeletal structures by micro-computed tomography (microCT). Bone mineral density was calculated by calibrating pixel x-ray attenuation along the skull of scanned individuals, relative to 0.25 and 0.75 g.cm^3 calcium hydroxyapatite phantoms, at 8 months post-fertilisation. Consistently, mineral density in the dermal bone of the skull was significantly increased in *golgb1*$^{Q2948X/Q2948X}$ fish compared to WT controls (Figure 5B-C). Furthermore, two out of three *golgb1*$^{Q2948X/Q2948X}$ adults showed ectopic calcium-like deposits close to the spinal cord (Figure 5D, E and Movies S3 and S4) or ribs, whilst the third had deposits within multiple vertebrae (Supplementary Movies S5 and S6). In addition to aberrant mineralization, HFTC is also associated with hyperostosis. WT and *golgb1*$^{Q2948X/Q2948X}$ fish had broadly indistinguishable skeletal structures, except for their craniofacial elements. Here we noted a narrowing and extension of ventral craniofacial cartilage as well as the bone

bioRxiv preprint doi: https://doi.org/10.1101/123547; this version posted April 3, 2017. The copyright holder for this preprint (which was not certified by peer review) is the author/funder, who has granted bioRxiv a license to display the preprint in perpetuity. It is made available under aCC-BY-NC-ND 4.0 International license.

243 elements of the mandible (Meckel's cartilage), palatoquadrate and ceratohyal, consistent with excessive

244 bone growth (Figures 5D, S3).

245

bioRxiv preprint doi: https://doi.org/10.1101/123547; this version posted April 3, 2017. The copyright holder for this preprint (which was not certified by peer review) is the author/funder, who has granted bioRxiv a license to display the preprint in perpetuity. It is made available under aCC-BY-NC-ND 4.0 International license.

Discussion

The data presented here demonstrate for the first time that the Golgi apparatus has the capacity to control its own composition. Specifically, we show that the enzymatic content of the Golgi is altered at the level of transcription in response to loss of giantin function. This process is conserved between mammalian cells and zebrafish models as GALNT3 mRNA is reduced in both giantin KO systems. Furthermore, we demonstrate functional and physiological relevance as giantin KO zebrafish show phenotypes consistent with the human congenital disorder of glycosylation, HFTC.

We report that 24 enzymes involved in multiple glycosylation pathways exhibit altered expression following GOLGB1 ablation. This implies that this change is not in response to a deficiency in a single reaction but a global adjustment of Golgi biochemistry. We consider this an adaptive response to giantin loss-of-function and it suggests a plasticity within the system that could have relevance to many processes including cell differentiation, tissue morphogenesis and responses to the extracellular environment. This is supported by the fact that KO cells and zebrafish are both viable and relatively unaffected by the transcriptional changes seen here. Indeed, lectin binding is largely equivalent in WT and KO cells suggesting that the new enzymatic equilibrium is broadly effective and the fidelity of glycosylation is largely maintained.

Genetic adaptation is an increasingly reported response to CRISPR/Cas9 generated mutations (Cerikan et al., 2016; Rossi et al., 2015). Such changes mask the original gene function but arguably better reflect disease states. We thus cannot retrospectively assess the immediate impact of GOLGB1 ablation in our system. Giantin depletion by siRNA, however, has been reported to cause the specific redistribution of Glucosaminyl (N-acetyl) transferase 3 (GCNT3) from the Golgi to the ER (Petrosyan et al., 2012). Expression of this gene was unaffected in our study but it is possible that perturbed transport of other enzymes instigated the transcriptional changes seen here. We found that giantin is not responsible for

bioRxiv preprint doi: https://doi.org/10.1101/123547; this version posted April 3, 2017. The copyright holder for this preprint (which was not certified by peer review) is the author/funder, who has granted bioRxiv a license to display the preprint in perpetuity. It is made available under aCC-BY-NC-ND 4.0 International license.

trafficking of GALNT3 to the Golgi, so transcriptional down-regulation of this enzyme at least is not the result of its mislocalisation.

Glycosylation is a seemingly robust process, with multiple compensatory mechanisms having been reported in response to gene loss. For example, loss of MGAT in T cells leads to the redistribution of sugar donors within Golgi cisternae to permit the synthesis of structurally dissimilar but bioequivalent glycans (Mkhikian et al., 2016). Interestingly, loss of MGAT expression does not result in major changes in the expression of other glycosyltransferases (Mkhikian et al., 2016). However, other work has shown that loss of one *N*-acetylglucosaminyltransferase can to lead to compensatory upregulation of a functionally equivalent isoform (Takamatsu et al., 2010). While these studies demonstrate the capacity of glycosylation for self-correction with respect to a single reaction, our data show for the first time the role of a non-enzymatic Golgi protein in global control of glycosylation.

The GALNT family of enzymes comprises extensive overlapping substrate specificities and so is a prime candidate for compensation (Bennett et al., 2012; Schjoldager et al., 2015). Indeed, five GALNTs are differentially expressed between WT and KO cells; GALNT1, GALNT3, GALNT12 and GALNT16 were down-regulated whilst GALNT5 was upregulated. Furthermore, staining with HPA lectin, which binds to the Tn antigen generated by GALNTs, was equivalent in WT and KO cell lines suggesting that the efficiency of this reaction was broadly maintained following these changes. Increased GALNT5 activity may therefore be sufficient to counter the loss of the other four enzymes, or the remaining GALNTs act collectively to ensure efficient *O*-glycosylation. The manifestation of HFTC-like phenotypes in giantin KO fish however is consistent with this idea that loss of GALNT3 cannot be fully compensated with respect to specific substrates. This contrasts with other work showing that deletion of either GALNT1 or GALNT2, or ectopic expression of GALNT3, does not result in substantial changes in expression of the other GALNTs (Schjoldager et al., 2015).

bioRxiv preprint doi: https://doi.org/10.1101/123547; this version posted April 3, 2017. The copyright holder for this preprint (which was not certified by peer review) is the author/funder, who has granted bioRxiv a license to display the preprint in perpetuity. It is made available under aCC-BY-NC-ND 4.0 International license.

The observed changes in expression of genes encoding Golgi-resident enzymes following loss of giantin expression suggests the existence of a Golgi-based quality control pathway for glycosylation. One interpretation of our data is that giantin itself is actively acting to monitor glycan synthesis or cargo transit and adjust gene expression accordingly. Such organelle-based signalling circuits are not without precedent; the nutrient sensor mTORC1 can interact with and phosphorylate transcription factor EB (TFEB) on the surface of lysosomes during starvation to promote its nuclear translocation (Settembre et al., 2012). Giantin itself lacks enzymatic activity but it could function as a signalling platform in this context. MAPK, PKD and PKA signalling have all been shown to regulate Golgi activity (Farhan and Rabouille, 2011) but whether any of these pathways intersect with giantin and transcription remains to be determined. No obvious trafficking defects were detected in the KO cells at steady state, consistent with a function independent of vesicle tethering. This agrees with a report showing that, unlike known tethers, mitochondrial relocation of giantin does not result in vesicle tethering to the mitochondrial membrane (Wong and Munro, 2014). Nonetheless the possibility remains that the control of intra-Golgi traffic by giantin acts to ensure the accurate distribution of enzymes across the stack and this intersects with a signalling loop that directs expression of glycosyltransferases.

Quality control mechanisms, such as may be active here, are well documented in the ER but to our knowledge only one study has looked at this specifically in the Golgi (Oku et al., 2011). This report found ten Golgi-relevant genes were upregulated in response to Golgi stress by virtue of a seven nucleotide cis-acting element within their promoters termed the Golgi apparatus stress response element (GASE) (Oku et al., 2011). We failed to identify these genes in our RNAseq analysis, nor was there any enrichment for promoters containing the GASE motif in our hits. It is therefore unlikely this pathway is active in our KO cells, but perhaps similar mechanisms exist to detect changes in the proteoglycome and adjust transcription accordingly.

bioRxiv preprint doi: https://doi.org/10.1101/123547; this version posted April 3, 2017. The copyright holder for this preprint (which was not certified by peer review) is the author/funder, who has granted bioRxiv a license to display the preprint in perpetuity. It is made available under aCC-BY-NC-ND 4.0 International license.

315 The lack of major structural changes in the Golgi apparatus in our KO cells is consistent with mouse KO
316 models (Lan et al., 2016) and knockdown systems (Asante et al., 2013; Koreishi et al., 2013). It has been
317 reported that the introduction of giantin into *Drosophila* S2 cells promotes clustering of Golgi stacks into
318 pseudo-ribbons, implying a role in lateral tethering (Koreishi et al., 2013). If this is the case, then the lack
319 of Golgi fragmentation in our KO models indicates that other golgins might fulfil this function in
320 vertebrate systems. One notable phenotype that we observed was the presence of circularized Golgi
321 structures following nocodazole treatment in giantin KO cells. This is counter-intuitive to a role in lateral
322 tethering since removal of an inter-cisternal tether should reduce, rather than encourage, interactions
323 between cisternal rims. Considering giantin has a predicted reach of 450nm into the cytosol it is possible
324 that instead it blocks interaction between similar membranes. During ribbon assembly, it would then
325 need to be excluded from the rims of the stacks that are coming together. Alternatively, it may play a
326 structural role in maintaining flat cisternae through homo- or heterotypic interactions. We only see
327 these circular structures following disassembly, suggesting larger Golgi ribbon structures may be under
328 other physical constraints that maintain its linear conformation. If giantin does have a role in
329 maintaining cisternal structure, changes in protein localisation or lipid packing in its absence could play a
330 role in controlling glycosyltransferase expression. Relocation of GM130 to larger Golgi elements in
331 nocodazole-treated giantin KO cells is consistent with its accumulation on the 'old Golgi' and with at
332 least a partial compensation of function following loss of giantin.

333 Considerable variation exists between giantin KO animal models (Bergen et al., 2017; Katayama et al.,
334 2011; Lan et al., 2016). All, however, exhibit defects that could be attributed to changes in glycosylation
335 affecting extracellular matrix deposition (Stanley, 2016; Tran and Ten Hagen, 2013). Changes in this
336 process due to altered glycosyltransferase expression could thus underlie the broad chondrogenesis and
337 osteogenesis phenotypes seen in rodent knockout animals, whilst the diversity seen with regards to
338 phenotypes likely reflects model specific modes of adaptation. The latter will be determined by tissue

bioRxiv preprint doi: https://doi.org/10.1101/123547; this version posted April 3, 2017. The copyright holder for this preprint (which was not certified by peer review) is the author/funder, who has granted bioRxiv a license to display the preprint in perpetuity. It is made available under aCC-BY-NC-ND 4.0 International license.

specific expression patterns, different developmental pathways, or differing compensatory mechanisms to produce bioequivalent glycans between species. Unlike our zebrafish mutants, HFTC phenotypes have not been reported in rodent giantin KO models however these animals die at birth prior to disease onset, whilst adult KO zebrafish are viable.

Overall, our work identifies a previously uncharacterised mechanism through which the Golgi can regulate its own biochemistry to produce a functional proteoglycome. Understanding the ability of cells to adapt and modulate glycosylation pathways through long term changes in gene expression has implications for normal development and disease pathogenesis in diverse contexts including congenital disorders of glycosylation (Jaeken, 2010), the onset and progression of cancer (Pinho and Reis, 2015), and long term health in terms of tissue regeneration and repair.

bioRxiv preprint doi: https://doi.org/10.1101/123547; this version posted April 3, 2017. The copyright holder for this preprint (which was not certified by peer review) is the author/funder, who has granted bioRxiv a license to display the preprint in perpetuity. It is made available under aCC-BY-NC-ND 4.0 International license.

Author contributions

NLS designed and performed experiments, analysed data and wrote the paper, DJB designed and performed experiments, analysed data and helped write the paper, RS helped with the zebrafish experiments, KARB performed and analysed microCT experiments. CLH helped to design experiments, interpret data and write the paper. DJS conceived and managed the project, contributed to data analysis, and helped to write the paper.

Acknowledgements

We would like to thank Franck Perez and Gaelle Boncompain for sharing the RUSH system with us, the Earlham Institute for the RNAseq analysis, Emily Wyatt for her contribution to the project and Andrew Herman and the UoB flow cytometry facility for help with cell sorting. Thanks to Martin Lowe for sharing reagents and for helpful discussions. We also thank the MRC and Wolfson Foundation for establishing the Wolfson Bioimaging Facility, and confocal microscopy was supported by a BBSRC ALERT 13 capital grant (BB/L014181/1). The project was funded by the MRC (MR/K018019/1), Wellcome Trust (099848/Z/12/Z), and Arthritis Research UK (19476 and 21211).

bioRxiv preprint doi: https://doi.org/10.1101/123547; this version posted April 3, 2017. The copyright holder for this preprint (which was not certified by peer review) is the author/funder, who has granted bioRxiv a license to display the preprint in perpetuity. It is made available under aCC-BY-NC-ND 4.0 International license.

References

Alvarez, C., Garcia-Mata, R., Hauri, H.P., and Sztul, E. (2001). The p115-interactive proteins GM130 and giantin participate in endoplasmic reticulum-Golgi traffic. J Biol Chem *276*, 2693-2700.

Asante, D., Maccarthy-Morrogh, L., Townley, A.K., Weiss, M.A., Katayama, K., Palmer, K.J., Suzuki, H., Westlake, C.J., and Stephens, D.J. (2013). A role for the Golgi matrix protein giantin in ciliogenesis through control of the localization of dynein-2. J Cell Sci *126*, 5189-5197.

Bard, F., and Chia, J. (2016). Cracking the Glycome Encoder: Signaling, Trafficking, and Glycosylation. Trends Cell Biol *26*, 379-388.

Beecham, G.W., Hamilton, K., Naj, A.C., Martin, E.R., Huentelman, M., Myers, A.J., Corneveaux, J.J., Hardy, J., Vonsattel, J.P., Younkin, S.G.*, et al.* (2014). Genome-wide association meta-analysis of neuropathologic features of Alzheimer's disease and related dementias. PLoS Genet *10*, e1004606.

Bennett, E.P., Mandel, U., Clausen, H., Gerken, T.A., Fritz, T.A., and Tabak, L.A. (2012). Control of mucin-type O-glycosylation: a classification of the polypeptide GalNAc-transferase gene family. Glycobiology *22*, 736-756.

Bergen, D.J., Stevenson, N.L., Skinner, R.J., Stephens, D.J., and Hammond, C.L. (2017). The Golgi matrix protein giantin is required for normal cilia function in zebrafish. bioRxiv.

Boncompain, G., Divoux, S., Gareil, N., de Forges, H., Lescure, A., Latreche, L., Mercanti, V., Jollivet, F., Raposo, G., and Perez, F. (2012). Synchronization of secretory protein traffic in populations of cells. Nature methods *9*, 493-498.

Brodsky, J.L. (2012). Cleaning up: ER-associated degradation to the rescue. Cell *151*, 1163-1167.

Cerikan, B., Shaheen, R., Colo, G.P., Glasser, C., Hata, S., Knobeloch, K.P., Alkuraya, F.S., Fassler, R., and Schiebel, E. (2016). Cell-Intrinsic Adaptation Arising from Chronic Ablation of a Key Rho GTPase Regulator. Dev Cell *39*, 28-43.

bioRxiv preprint doi: https://doi.org/10.1101/123547; this version posted April 3, 2017. The copyright holder for this preprint (which was not certified by peer review) is the author/funder, who has granted bioRxiv a license to display the preprint in perpetuity. It is made available under aCC-BY-NC-ND 4.0 International license.

390 Farhan, H., and Rabouille, C. (2011). Signalling to and from the secretory pathway. J Cell Sci *124*, 171-
391 180.
392 Fourriere, L., Divoux, S., Roceri, M., Perez, F., and Boncompain, G. (2016). Microtubule-independent
393 secretion requires functional maturation of Golgi elements. J Cell Sci *129*, 3238-3250.
394 Freeze, H.H., and Ng, B.G. (2011). Golgi glycosylation and human inherited diseases. Cold Spring Harb
395 Perspect Biol *3*, a005371.
396 Gillingham, A.K., and Munro, S. (2016). Finding the Golgi: Golgin Coiled-Coil Proteins Show the Way.
397 Trends Cell Biol *26*, 399-408.
398 Ichikawa, S., Guigonis, V., Imel, E.A., Courouble, M., Heissat, S., Henley, J.D., Sorenson, A.H., Petit, B.,
399 Lienhardt, A., and Econs, M.J. (2007). Novel GALNT3 mutations causing hyperostosis-
400 hyperphosphatemia syndrome result in low intact fibroblast growth factor 23 concentrations. J Clin
401 Endocrinol Metab *92*, 1943-1947.
402 Jaeken, J. (2010). Congenital disorders of glycosylation. Ann N Y Acad Sci *1214*, 190-198.
403 Katayama, K., Sasaki, T., Goto, S., Ogasawara, K., Maru, H., Suzuki, K., and Suzuki, H. (2011). Insertional
404 mutation in the Golgb1 gene is associated with osteochondrodysplasia and systemic edema in the OCD
405 rat. Bone *49*, 1027-1036.
406 Kato, K., Jeanneau, C., Tarp, M.A., Benet-Pages, A., Lorenz-Depiereux, B., Bennett, E.P., Mandel, U.,
407 Strom, T.M., and Clausen, H. (2006). Polypeptide GalNAc-transferase T3 and familial tumoral calcinosis.
408 Secretion of fibroblast growth factor 23 requires O-glycosylation. J Biol Chem *281*, 18370-18377.
409 Kimmel, C.B., Ballard, W.W., Kimmel, S.R., Ullmann, B., and Schilling, T.F. (1995). Stages of embryonic
410 development of the zebrafish. Developmental dynamics : an official publication of the American
411 Association of Anatomists *203*, 253-310.

bioRxiv preprint doi: https://doi.org/10.1101/123547; this version posted April 3, 2017. The copyright holder for this preprint (which was not certified by peer review) is the author/funder, who has granted bioRxiv a license to display the preprint in perpetuity. It is made available under aCC-BY-NC-ND 4.0 International license.

412 Koreishi, M., Gniadek, T.J., Yu, S., Masuda, J., Honjo, Y., and Satoh, A. (2013). The golgin tether giantin
413 regulates the secretory pathway by controlling stack organization within Golgi apparatus. PLoS ONE *8*,
414 e59821.
415 Lan, Y., Zhang, N., Liu, H., Xu, J., and Jiang, R. (2016). Golgb1 regulates protein glycosylation and is crucial
416 for mammalian palate development. Development *143*, 2344-2355.
417 Linstedt, A.D., and Hauri, H.P. (1993). Giantin, a novel conserved Golgi membrane protein containing a
418 cytoplasmic domain of at least 350 kDa. Mol Biol Cell *4*, 679-693.
419 Mkhikian, H., Mortales, C.L., Zhou, R.W., Khachikyan, K., Wu, G., Haslam, S.M., Kavarian, P., Dell, A., and
420 Demetriou, M. (2016). Golgi self-correction generates bioequivalent glycans to preserve cellular
421 homeostasis. Elife *5*.
422 Ng, M.C., Hester, J.M., Wing, M.R., Li, J., Xu, J., Hicks, P.J., Roh, B.H., Lu, L., Divers, J., Langefeld, C.D.*, et*
423 *al.* (2012). Genome-wide association of BMI in African Americans. Obesity (Silver Spring) *20*, 622-627.
424 Nizak, C., Martin-Lluesma, S., Moutel, S., Roux, A., Kreis, T.E., Goud, B., and Perez, F. (2003).
425 Recombinant antibodies against subcellular fractions used to track endogenous Golgi protein dynamics
426 in vivo. Traffic *4*, 739-753.
427 Oku, M., Tanakura, S., Uemura, A., Sohda, M., Misumi, Y., Taniguchi, M., Wakabayashi, S., and Yoshida,
428 H. (2011). Novel cis-acting element GASE regulates transcriptional induction by the Golgi stress
429 response. Cell Struct Funct *36*, 1-12.
430 Petrosyan, A., Ali, M.F., and Cheng, P.W. (2012). Glycosyltransferase-specific Golgi-targeting
431 mechanisms. J Biol Chem *287*, 37621-37627.
432 Pinho, S.S., and Reis, C.A. (2015). Glycosylation in cancer: mechanisms and clinical implications. Nat Rev
433 Cancer *15*, 540-555.

bioRxiv preprint doi: https://doi.org/10.1101/123547; this version posted April 3, 2017. The copyright holder for this preprint (which was not certified by peer review) is the author/funder, who has granted bioRxiv a license to display the preprint in perpetuity. It is made available under aCC-BY-NC-ND 4.0 International license.

Ran, F.A., Hsu, P.D., Lin, C.Y., Gootenberg, J.S., Konermann, S., Trevino, A.E., Scott, D.A., Inoue, A., Matoba, S., Zhang, Y.*, et al.* (2013). Double nicking by RNA-guided CRISPR Cas9 for enhanced genome editing specificity. Cell *154*, 1380-1389.

Rosing, M., Ossendorf, E., Rak, A., and Barnekow, A. (2007). Giantin interacts with both the small GTPase Rab6 and Rab1. Exp Cell Res *313*, 2318-2325.

Rossi, A., Kontarakis, Z., Gerri, C., Nolte, H., Holper, S., Kruger, M., and Stainier, D.Y. (2015). Genetic compensation induced by deleterious mutations but not gene knockdowns. Nature *524*, 230-233.

Schjoldager, K.T., Joshi, H.J., Kong, Y., Goth, C.K., King, S.L., Wandall, H.H., Bennett, E.P., Vakhrushev, S.Y., and Clausen, H. (2015). Deconstruction of O-glycosylation--GalNAc-T isoforms direct distinct subsets of the O-glycoproteome. EMBO Rep *16*, 1713-1722.

Settembre, C., Zoncu, R., Medina, D.L., Vetrini, F., Erdin, S., Erdin, S., Huynh, T., Ferron, M., Karsenty, G., Vellard, M.C.*, et al.* (2012). A lysosome-to-nucleus signalling mechanism senses and regulates the lysosome via mTOR and TFEB. Embo J *31*, 1095-1108.

Sohda, M., Misumi, Y., Yamamoto, A., Yano, A., Nakamura, N., and Ikehara, Y. (2001). Identification and characterization of a novel Golgi protein, GCP60, that interacts with the integral membrane protein giantin. J Biol Chem *276*, 45298-45306.

Sönnichsen, B., Lowe, M., Levine, T., Jämsä, E., Dirac-Svejstrup, B., and Warren, G. (1998). A role for giantin in docking COPI vesicles to Golgi membranes. J Cell Biol *140*, 1013-1021.

Stanley, P. (2016). What Have We Learned from Glycosyltransferase Knockouts in Mice? J Mol Biol *428*, 3166-3182.

Takamatsu, S., Antonopoulos, A., Ohtsubo, K., Ditto, D., Chiba, Y., Le, D.T., Morris, H.R., Haslam, S.M., Dell, A., Marth, J.D.*, et al.* (2010). Physiological and glycomic characterization of N-acetylglucosaminyltransferase-IVa and -IVb double deficient mice. Glycobiology *20*, 485-497.

bioRxiv preprint doi: https://doi.org/10.1101/123547; this version posted April 3, 2017. The copyright holder for this preprint (which was not certified by peer review) is the author/funder, who has granted bioRxiv a license to display the preprint in perpetuity. It is made available under aCC-BY-NC-ND 4.0 International license.

457 Thyberg, J., and Moskalewski, S. (1985). Microtubules and the organization of the Golgi complex. Exp
458 Cell Res *159*, 1-16.
459 Topaz, O., Shurman, D.L., Bergman, R., Indelman, M., Ratajczak, P., Mizrachi, M., Khamaysi, Z., Behar, D.,
460 Petronius, D., Friedman, V.*, et al.* (2004). Mutations in GALNT3, encoding a protein involved in O-linked
461 glycosylation, cause familial tumoral calcinosis. Nat Genet *36*, 579-581.
462 Tran, D.T., and Ten Hagen, K.G. (2013). Mucin-type O-glycosylation during development. J Biol Chem
463 *288*, 6921-6929.
464 Westerfield, M. (2000). The zebrafish book. A guide for the laboratory use of zebrafish (Danio rerio). Vol
465 4th ed.
466 Wong, M., and Munro, S. (2014). The specificity of vesicle traffic to the Golgi is encoded in the golgin
467 coiled-coil proteins. Science *346*, 1256898.
468 Yang, W., and Storrie, B. (1998). Scattered Golgi elements during microtubule disruption are initially
469 enriched in trans-Golgi proteins. Mol Biol Cell *9*, 191-207.

470

471

bioRxiv preprint doi: https://doi.org/10.1101/123547; this version posted April 3, 2017. The copyright holder for this preprint (which was not certified by peer review) is the author/funder, who has granted bioRxiv a license to display the preprint in perpetuity. It is made available under aCC-BY-NC-ND 4.0 International license.

Materials and Methods

All reagents were purchased from Sigma-Aldrich unless stated otherwise.

Method details

Cell culture

Human telomerase-immortalised retinal pigment epithelial cells (hTERT-RPE1, Takara Bio) were grown in DMEM-F12 supplemented with 10% FCS (Life Technologies, Paisley, UK). Cell lines were not authenticated after purchase other than confirming absence of mycoplasma contamination.

Transfections were performed using Lipofectamine 2000™ according to the manufacturer's instructions (Invitrogen, Carlsbad, CA). Flag-GALNT3 was obtained from ViGene Biosciences (Cat# CH897457, Rockville, MD) Str-Kdel/Man-SBP-EGFP was a gift from Franck Perez (Institut Curie, Paris, (Boncompain et al., 2012)). For drug treatments cells were incubated with 5 µM nocodazole (Santa Cruz, Heidelberg, Germany) or 5 µM brefeldin A diluted in growth medium at 37^{o}C then washed 3x with growth medium for recovery.

Zebrafish husbandry and mutant alleles

London AB zebrafish were used and maintained according to standard conditions (Westerfield, 2000) and staged accordingly (Kimmel et al., 1995). Ethical approval was obtained from the University of Bristol Ethical Review Committee using the Home Office Project License number 30/2863. The *golgb1*^{Q2948X} and *golgb1*^{3078X} alleles are described in (Bergen et al., 2017).

CRISPR

RPE1 cells were transfected as above with 1µg each of paired gRNAs HSL0001186601 (ACCTGAGCACGGCCCACCAAGG) and HSR0001186603 (GTCGTTGACTTGCTGCAACAGG) (obtained from Sigma) targeting the GOLGB1 gene plus 0.1 µg pSpCas9n(BB)-2A-GFP (Addgene plasmid #48140 PX461

bioRxiv preprint doi: https://doi.org/10.1101/123547; this version posted April 3, 2017. The copyright holder for this preprint (which was not certified by peer review) is the author/funder, who has granted bioRxiv a license to display the preprint in perpetuity. It is made available under aCC-BY-NC-ND 4.0 International license.

(Ran et al., 2013)). After 48 hours GFP-positive cells were sorted into 96 well plates, seeding one cell per well to generate clones. To identify mutations, genomic DNA was prepared using a Purelink® genomic DNA mini kit (Invitrogen, Carlsbad, CA) and the region targeted by the gRNAs amplified by PCR (primers: forward 5'-CTGGGTCTGGTTGTTGTTGGT-3' reverse 5'-GGTGTCATGTTGGTGCTCAG-3'; reaction mix: Taq DNA polymerase with thermopol® buffer, 10mM dNTP mix, 10µM each primer and 2µl genomic DNA; reagents from NEB (M0267L, N0447L); program: 94°C 5 min, 18 cycle touchdown PCR from 58-48°C followed by 22 cycles at 48°C - each cycle 25 s melting step at 94°C, 25 s annealing at x°C and 68°C 65 s extension - then a 5 minute final annealing step at 68°C and 10°C hold). PCR products were cloned into the pGEM® T Easy vector according to the manufacturer's instructions and sequenced using predesigned primers against the T7 promoter (MWG Eurofins).

Antibodies, labelling and microscopy

Antibodies used: mouse monoclonal anti-giantin (full length, Abcam, Cambridge, UK, ab37266), rabbit polyclonal anti-giantin (N-terminus, Covance, CA, PRB-114C), rabbit polyclonal anti-giantin (C-term, gift from Martin Lowe), mouse anti-GM130 and mouse GMAP210 (BD Biosciences, Oxford, UK, BD 610823 & BD 611712), sheep anti-TGN46 (Bio-Rad, Hertfordshire, UK, AHP500), sheep anti-GRASP65 (gift from Jon Lane), sec23a (homemade, polyclonal), mouse ERGIC53 (monoclonal clone G1/93, Alexis Biochemicals, ALX-804-602-C100), TFG (Novus Biologicals, Cambridge, UK), Sec16A (KIAA0310, Bethyl Labs, Montgomery, TX, A300-648A), ER stress antibody sampler kit (Cell Signalling, Hertfordshire, UK, 9956), mouse anti-tubulin and rabbit polyclonal anti-FLAG (Sigma, Dorset, UK, T5168 & F7425), CASP (gift from Sean Munro), mouse anti-GAPDH (Abcam, Cambridge, UK, ab9484), rabbit anti-CHST11 (Proteintech, Manchester, UK, 15959-1-AP). Lectins used: HPA biotinylated lectin (Fisher Scientific, Loughborough, UK, L11271), Biotinylated lectin kit I (Vector laboratories, Peterborough UK, BK-1000). HABP (Merck, Hertfordshire, UK, 385911).

bioRxiv preprint doi: https://doi.org/10.1101/123547; this version posted April 3, 2017. The copyright holder for this preprint (which was not certified by peer review) is the author/funder, who has granted bioRxiv a license to display the preprint in perpetuity. It is made available under aCC-BY-NC-ND 4.0 International license.

For antibody labelling, cells were grown on autoclaved coverslips (Menzel #1.5, Fisher Scientific, Loughborough, UK), rinsed with PBS and fixed in MeOH for 4 minutes at -20°C. Cells were then blocked in 3% BSA-PBS for 30 minutes and incubated with primary then secondary antibody for 1 hour each, washing in between. Nuclei were stained with DAPI [4,6-diamidino-2-phenylindole (Life Technologies, Paisley, UK, D1306)] for 3 minutes and coverslips mounted in Mowiol (MSD, Hertfordshire, UK) or Prolong Diamond antifade (Thermo Fisher, Paisley, UK). For lectin labelling, cells were washed in PBS and fixed in 3% PFA-PBS for 10 minutes at room temperature (for lectins) or 10 minutes on ice plus 10 minutes at room temperature (for HABP). Cells were permeabilised in 1% (lectins) or 0.1% (HABP) TTX-100 in PBS and blocked as above. Biotinylated lectins were diluted to 4 µg/ml in block and incubated with cells for 40 minutes whilst HAPB was diluted to 5 µg/ml and incubated overnight at 4°C. Cells were washed with PBS, incubated with giantin antibody for 15 minutes, washed and labelled with streptavidin-A568 and anti-rabbit A488 (Fisher Scientific, Loughborough, UK, S11226). Cells were DAPI stained and mounted as above.

Fixed cells were imaged using an Olympus IX70 microscope with 60x 1.42 NA oil-immersion lens, Exfo 120 metal halide illumination with excitation, dichroic and emission filters (Semrock, Rochester, NY), and a Photometrics Coolsnap HQ2 CCD, controlled by Volocity 5.4.1 (Perkin Elmer, Seer Green, UK). Chromatic shifts in images were registration corrected using TetraSpek fluorescent beads (Thermo Fisher). Images were acquired as 0.2µm z-stacks unless otherwise stated in the figure legend.

For RUSH assays, cells were seeded onto 35-mm glass-bottomed dishes (MatTek, Ashland, MA) or coverslips and transfected 24 hr prior to assay; at T0 cells were treated with 40 µM biotin then imaged every 15 seconds as a single plane for up to 1 hr or fixed at specific time points and stained as above. Live widefield microscopy proceeded using an Olympus IX81 microscope with 60x 1.42 numerical aperture oil-immersion lens, Sutter DG4 illumination with excitation filters, and multi-pass dichoric and

bioRxiv preprint doi: https://doi.org/10.1101/123547; this version posted April 3, 2017. The copyright holder for this preprint (which was not certified by peer review) is the author/funder, who has granted bioRxiv a license to display the preprint in perpetuity. It is made available under aCC-BY-NC-ND 4.0 International license.

multi-pass emission filters (Semrock). Images were collected using an Orca Flash 2.8 sCMOS controlled using Volocity 5.4.2 (PerkinElmer). Cells were kept at 37°C for the duration of the imaging.

Quantification of Golgi structure from widefield images was performed using ImageJ software. Maximum projection images (GRASP65 channel) were generated from 0.2µm z-stacks and thresholded before applying the analyse particles feature excluding objects <0.5µm^2 or on the edge of the field of view. Golgi cisternal length and curvature measurements taken from micrographs were again made with ImageJ using the segmented line and angle tools. Cisternae number and RUSH experiments were quantified manually and blind.

EM

Cells were fixed in 2.5% glutaraldehyde, washed for 5 minutes in 0.1M cacodylate buffer then post-fixed in 1% OsO4/0.1 M cacodylate buffer for 30 minutes. Cells were washed 3x with water and stained with 3% uranyl acetate for 20 minutes. After another rinse with water, cells were dehydrated by sequential 10 minute incubations with 70, 80, 90, 96, 100 and 100% EtOH before embedding in Epon™ at 70°C for 48 hours. Thin 70nm serial sections were cut and stained with 3% uranyl acetate then lead citrate, washing 3x with water after each. Once dried, sections were imaged using a FEI Tecnai12.

Immunoblotting

Cells were lysed in RIPA buffer (50 mM Tris pH7.5, 300 mM NaCl, 2% Triton-X100, 1% deoxycholate, 0.1% SDS, 1 mM EDTA) and samples separated by SDS-PAGE followed by transfer to nitrocellulose membranes. Membranes were blocked in 5% milk-TBST or 3% BSA-TBST for antibody and lectin probes respectively. Primary antibodies/lectins diluted in block were incubated with membrane overnight and detected using HRP-conjugated secondary antibodies or streptavidin respectively (Jackson ImmunoResearch, West Grove, PA) and enhanced chemiluminescence (GE Healthcare, Cardiff, United Kingdom).

bioRxiv preprint doi: https://doi.org/10.1101/123547; this version posted April 3, 2017. The copyright holder for this preprint (which was not certified by peer review) is the author/funder, who has granted bioRxiv a license to display the preprint in perpetuity. It is made available under aCC-BY-NC-ND 4.0 International license.

Quantitative PCR

Total RNA was isolated from ventral bone and cartilage of juvenile *golgb1*^{Q2948X} and *golgb1*^{3078X} genotyped fish (30 dpf, n=3 per genotype) using RNeasy mini kit (cat# 74104, Qiagen, Manchester, UK). Subsequently, a reverse transcriptase reaction was performed by using SuperscriptIV (cat# 18091050, Thermo Fisher). Zebrafish *galnt3* (XM_009300463.2) coding sequence was confirmed by multi-species nucleotide BLAST (NCBI) leading to *galnt3* forward 5'-TCCTTCAGAGTGTGGCAGTG and reverse 5'-TGATGGTGTTGTGGCCTTTA primers. *gapdh* as a reference gene was used forward 5'-TGTTCCAGTACGACTCCACC and reverse 3'- GCCATACCAGTAAGCTTGCC. Quantitative Real-Time PCR (qPCR) reactions (quadruplicates per individual) using DyNAmo HS SYBR green (F410L, Thermo Fisher) with PCR cycles (40 times) of 95°C 25 seconds, 57.5°C 30 second, and 70°C 45 seconds followed by a standard melt curve were applied (QuantStudio3, Applied Biosystems).

RNAseq

Triplicate samples of mRNA from giantin knockout cells and WT RPE1 were analysed by RNAseq by the Earlham Institute (formerly The Genome Analysis Centre). The libraries were constructed by The Earlham Institute on a PerkinElmer Sciclone using the TruSeq RNA protocol v2 (Illumina 15026495 Rev.F). The library preparation involved the initial QC of the RNA using a Tecan plate reader with the Quant-iT™ RNA Assay Kit (Life technologies/Invitrogen Q-33140) and the Quant-iT™ DNA Assay Kit, high sensitivity (Life technologies/Invitrogen Q-33120). Finally, the quality of the RNA was established using the PerkinElmer GX with a high sensitivity chip and High Sensitivity DNA reagents (PerkinElmer 5067-4626). RNA quality scores were 8.7 and 9.8 for two of the samples and 10.0 (for the remaining 4 samples). 1 ug of RNA was purified to extract mRNA with a poly- A pull down using biotin beads, fragmented and first strand cDNA was synthesised. This process reverse transcribes the cleaved RNA fragments primed with random hexamers into first strand cDNA using reverse transcriptase and random

bioRxiv preprint doi: https://doi.org/10.1101/123547; this version posted April 3, 2017. The copyright holder for this preprint (which was not certified by peer review) is the author/funder, who has granted bioRxiv a license to display the preprint in perpetuity. It is made available under aCC-BY-NC-ND 4.0 International license.

primers. The ends of the samples were repaired using the 3' to 5' exonuclease activity to remove the 3' overhangs and the polymerase activity to fill in the 5' overhangs creating blunt ends. A single 'A' nucleotide was added to the 3' ends of the blunt fragments to prevent them from ligating to one another during the adapter ligation reaction. A corresponding single 'T' nucleotide on the 3' end of the adapter provided a complementary overhang for ligating the adapter to the fragment. This strategy ensured a low rate of chimera formation. The ligation of a number indexing adapters to the ends of the DNA fragments prepared them for hybridisation onto a flow cell. The ligated products were subjected to a bead based size selection using Beckman Coulter XP beads (Beckman Coulter A63880) to remove un-ligated adapters, as well as any adapters that may have ligated to one another. Prior to hybridisation to the flow cell the samples were amplified by PCR to selectively enrich those DNA fragments that have adapter molecules on both ends and to amplify the amount of DNA in the library. The PCR was performed with a PCR primer cocktail that annealed to the ends of the adapter. The insert size of the libraries was verified by running an aliquot of the DNA library on a PerkinElmer GX using the High Sensitivity DNA chip and reagents (PerkinElmer CLS760672) and the concentration was determined by using the Tecan plate reader. The resulting libraries were then equimolar pooled and Q-PCR was performed on the pool prior to clustering.

These six total RNA samples were sequenced over two lanes and aligned against the human genome reference build 38 followed by differential expression analysis between the wildtype and knockout samples. QC was done using FastQC (fastqc version 0.11.2). An in-house contamination-screening pipeline (Kontaminant) was used to check for any obvious contamination in the raw reads. Since the data quality was good, there was no trimming done on the raw reads. Alignment of RNAseq reads to the human genome reference was done using TopHat (tophat version 2.1.0) with "min-anchor-length" 12 and "max-multi hits" 20. The $\log_2$ of the fold-change was used in further analysis.

bioRxiv preprint doi: https://doi.org/10.1101/123547; this version posted April 3, 2017. The copyright holder for this preprint (which was not certified by peer review) is the author/funder, who has granted bioRxiv a license to display the preprint in perpetuity. It is made available under aCC-BY-NC-ND 4.0 International license.

Micro-Computed Tomography Scanning (µCT)

Female fish (n=3) carrying *golgb1*$^{WT/WT}$ and mutant *golgb1*$^{Q2948X/Q2948X}$ alleles were preserved in absolute ethanol at 8 mpf. Prior to scanning, the samples were packed in a polystyrene tube and scanned with a Bruker SkyScan 1272 (Kontich, Belgium) at a 21.8 or 4 µm resolution. The X-ray current was set at 200 µA with a voltage of 50 kV. Skull bone mass density was assessed with CTAn software (v.1.15.1) measuring 6 points of 3x3 pixel size circles on 1 z-slice, repeated on 2 additional z-slices (20 z-steps apart) per individual. Sample pixel x-ray attenuation was correlated to a scan of a reference grid containing known calcium-phosphate concentration (0.25, and 0.75 g.cm^3 calcium hydroxyapatite). 3D tomography images and movies were generated using CTvox software (v.3.0.0).

Quantification and statistical analysis

Statistical analyses were performed using Graphpad Prism 7.00. The tests used, n numbers and sample sizes are indicated in the figure legends, p-values are shown on the figures.

Data and software availability

Raw RNAseq data are available in the ArrayExpress database (www.ebi.ac.uk/arrayexpress) under accession number E-MTAB-5618.

bioRxiv preprint doi: https://doi.org/10.1101/123547; this version posted April 3, 2017. The copyright holder for this preprint (which was not certified by peer review) is the author/funder, who has granted bioRxiv a license to display the preprint in perpetuity. It is made available under aCC-BY-NC-ND 4.0 International license.

Figure 1 – Generation of a giantin KO cell line. A. Genomic sequence for CRISPR-Cas9 target site in WT and engineered KO RPE1 cell line. Purple lines and scissors depict gRNA binding and cut sites. Blue nucleotides show the CRISPR PAM site. Green and red nucleotides are those deleted and inserted in the KO mutation respectively. Amino acid translation shown underneath; asterisk indicates a premature stop codon. B. Western blot analysis and C. immunofluorescence staining of giantin using three different antibodies raised against the C-terminus (C-term), N-terminus (N-term) and full length (FL) protein. All immunoreactivity is lost in the KO cells. D. WT and KO cell mixed population stained for giantin and other Golgi markers for direct comparison. Images are maximum projections. Scale bars 10µm.

bioRxiv preprint doi: https://doi.org/10.1101/123547; this version posted April 3, 2017. The copyright holder for this preprint (which was not certified by peer review) is the author/funder, who has granted bioRxiv a license to display the preprint in perpetuity. It is made available under aCC-BY-NC-ND 4.0 International license.

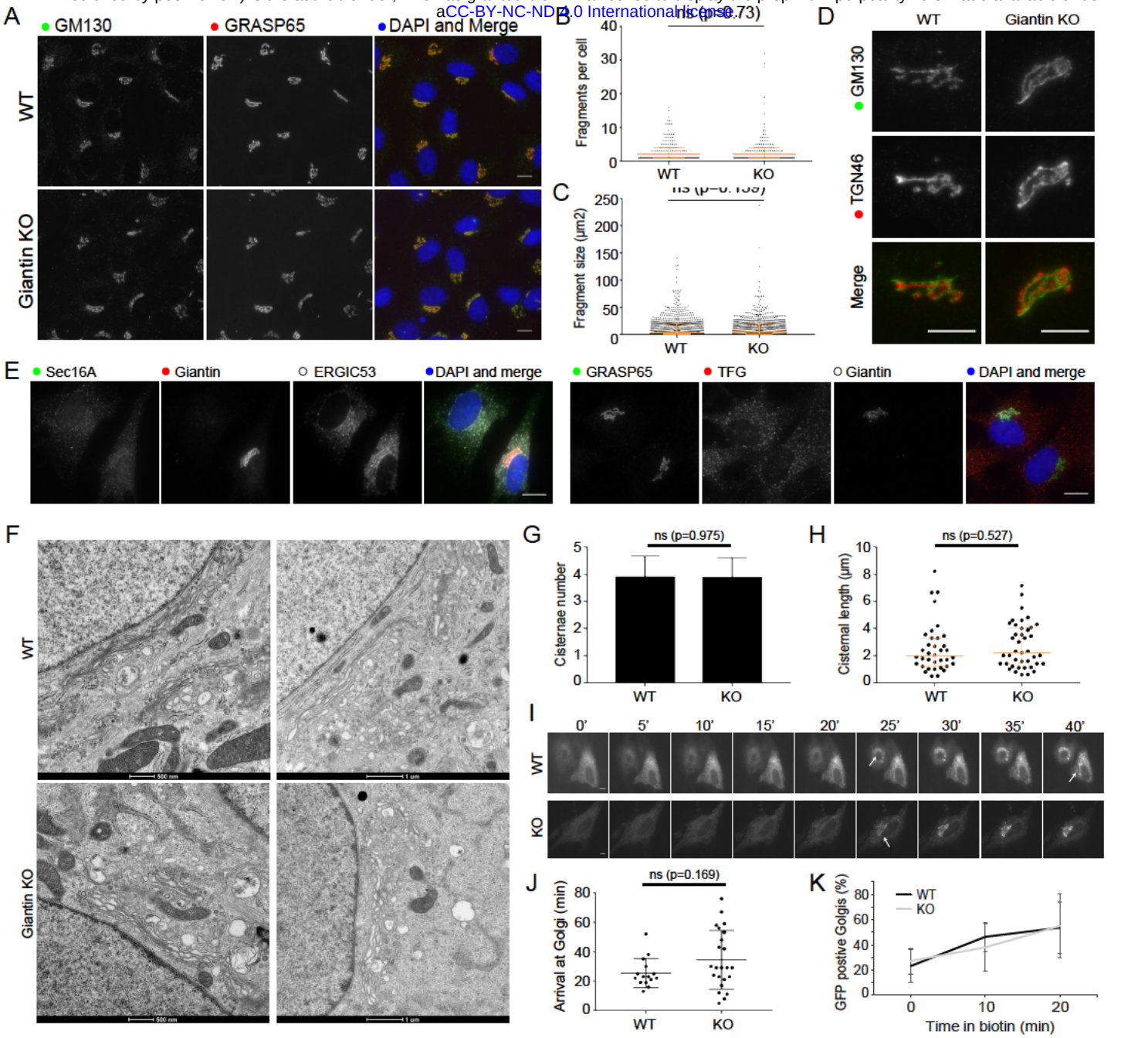

bioRxiv preprint doi: https://doi.org/10.1101/123547; this version posted April 3, 2017. The copyright holder for this preprint (which was not certified by peer review) is the author/funder, who has granted bioRxiv a license to display the preprint in perpetuity. It is made available under aCC-BY-NC-ND 4.0 International license.

Figure 2 – Loss of giantin has no effect on Golgi structure or trafficking. A. Representative images of WT and KO cells immuno-labelled for two cis-Golgi markers. The number of GM130 positive elements per cell (B) and their area (C) was found to be equivalent in WT and KO cells (n=3; 387 WT and 320 KO cells quantified; orange bars indicate median and interquartile range; statistics Mann-Whitney; fragments smaller than 0.5µm^2 excluded). D. Co-labelling of cells with cis- (GM130) and trans- (TGN46) Golgi markers shows Golgi polarity is maintained in KO cells. E. Representative images of WT and KO cells immuno-labelled for early secretory pathway markers as indicated. A-E. Images shown are maximum projections. Scale bar 10µm. F. Transmission electron micrographs of Golgi elements in WT and KO cells. The number of cisternae per stack (G) and length of Golgi cisternae (H) was quantified from experiments represented in (F) (n=3; total 30 cells per cell line; orange bars indicate median and interquartile range; statistics Mann-Whitney). I-L. WT and KO cells expressing Str-Kdel/ManI-SBP-EGFP were treated with biotin and imaged live (I-J) or fixed at 0, 10 and 20 minutes post-biotin addition and immuno-labelled for GM130 (K-L). I. Single plane images taken from representative movies at 5 minute intervals. See supplemental movies. Scale bar 10µm. Arrows show arrival of reporter at Golgi. J. Quantification of the time at which fluorescence appears in the Golgi apparatus in movies represented in (I) (n=3; 15 WT cells and 23 KO cells quantified; bars show median and interquartile range; statistics Mann-Whitney). K. Quantification of the number of GFP-positive Golgi at each timepoint in fixed cells (n=3; 378 WT and 310 KO cells quantified; mean and standard deviation shown; statistics ANOVA – all time points non-significant). L. Representative single plane images of fixed cells at each timepoint. G. Western blot analyses of ER stress markers in lysates taken from WT and KO cells following treatment with BFA for the indicated time.

bioRxiv preprint doi: https://doi.org/10.1101/123547; this version posted April 3, 2017. The copyright holder for this preprint (which was not certified by peer review) is the author/funder, who has granted bioRxiv a license to display the preprint in perpetuity. It is made available under aCC-BY-NC-ND 4.0 International license.

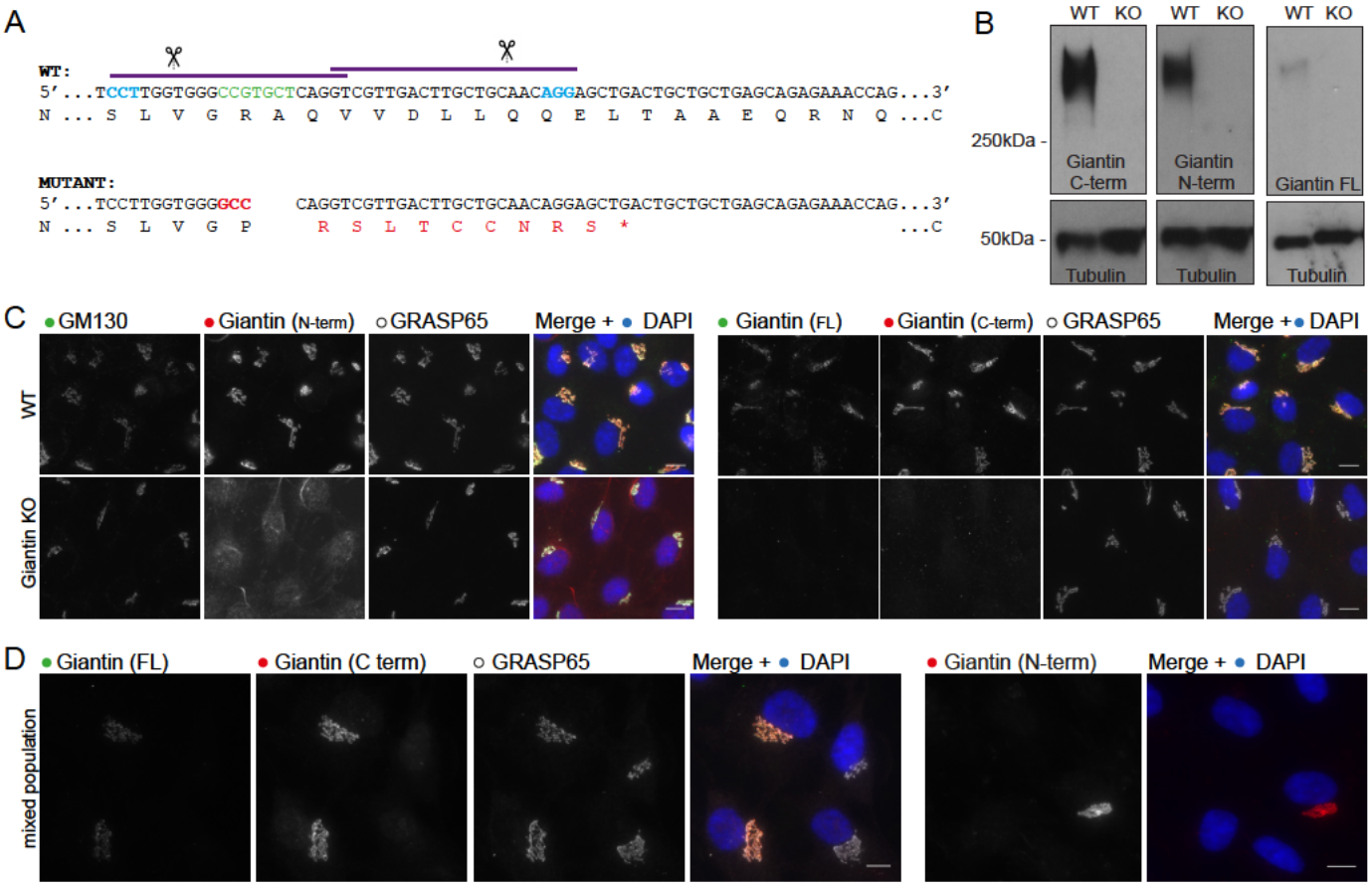

bioRxiv preprint doi: https://doi.org/10.1101/123547; this version posted April 3, 2017. The copyright holder for this preprint (which was not certified by peer review) is the author/funder, who has granted bioRxiv a license to display the preprint in perpetuity. It is made available under aCC-BY-NC-ND 4.0 International license.

Figure 3 – Giantin loss leads to mild changes in Golgi mini-stack structure. A. Representative maximum projection images of WT and giantin KO cells incubated with 5µm nocodazole as indicated and immuno-labelled for cis-(GM130) and trans-(TGN46) Golgi markers or tubulin. In wash out panels, cells were incubated with nocodazole for 3 hours then washed and incubated in growth medium for time indicated. Scale bars 10µm. B. Western blot analysis of golgin expression in WT and KO cells. C. Quantification of blots represented in (B) (n=3, mean and standard deviation shown). D. Transmission micrographs of WT and KO cells incubated with 5µm nocodazole for 90 minutes. Inserts show zoom of region denoted by black squares. E-G. Quantification of experiments represented in D showing (E) cisternal length, (F) number of cisternae per stack and (G) the angle between lines drawn from each lateral rim of the stack to the centre (n=3; 27 WT and 21 KO cells quantified; E and G show median and interquartile range, F mean and standard deviation; statistics Mann-Whitney).

bioRxiv preprint doi: https://doi.org/10.1101/123547; this version posted April 3, 2017. The copyright holder for this preprint (which was not certified by peer review) is the author/funder, who has granted bioRxiv a license to display the preprint in perpetuity. It is made available under aCC-BY-NC-ND 4.0 International license.

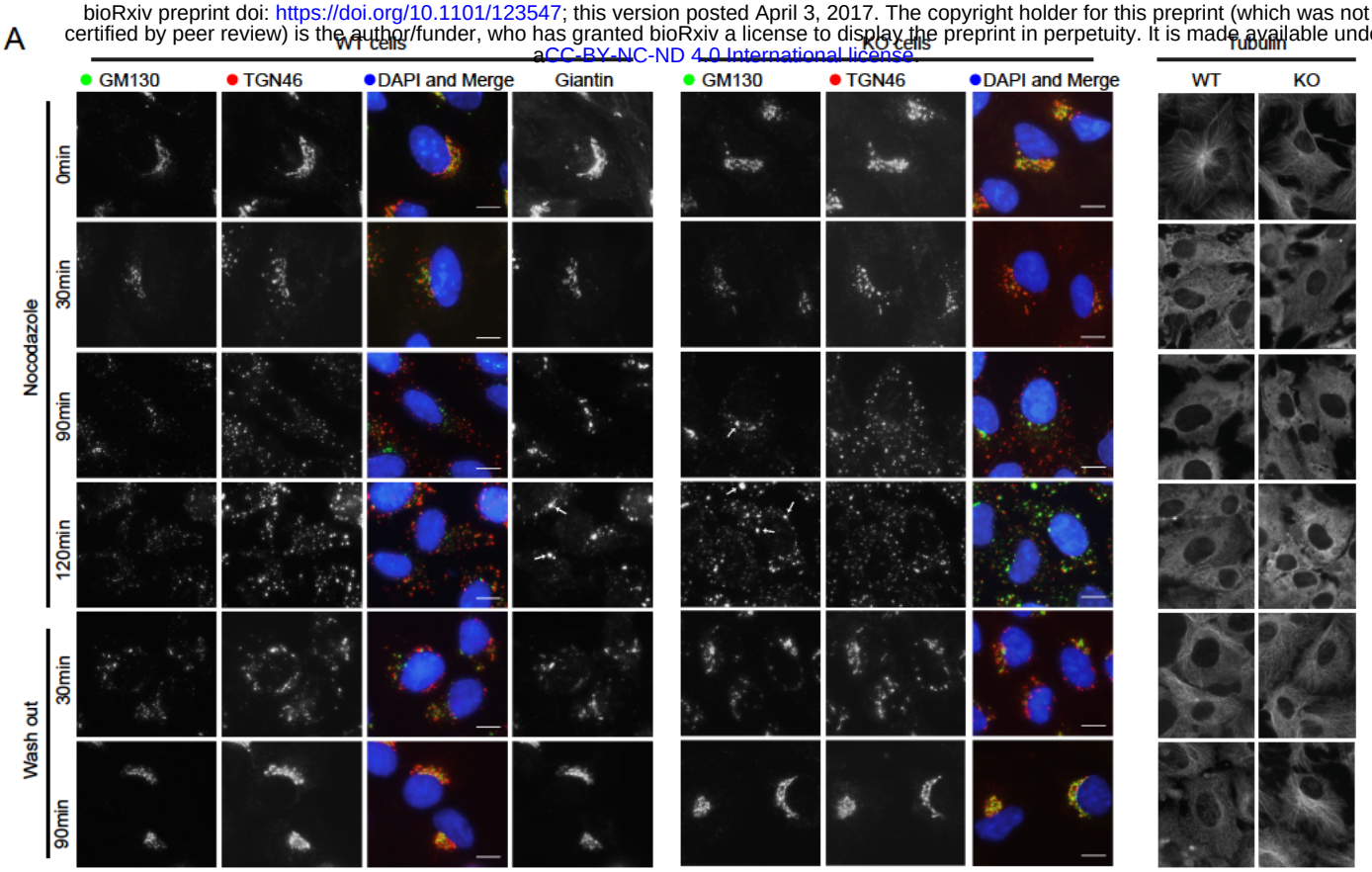

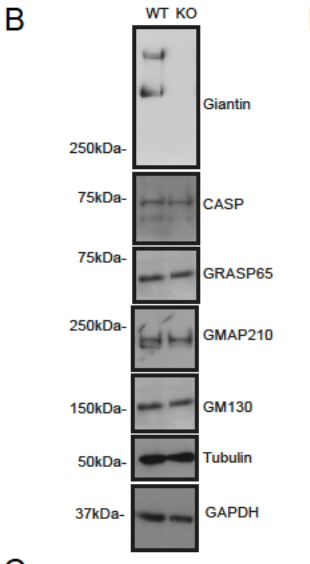

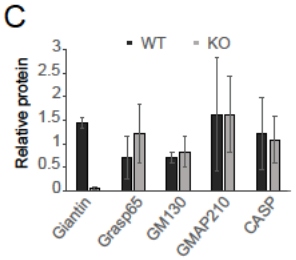

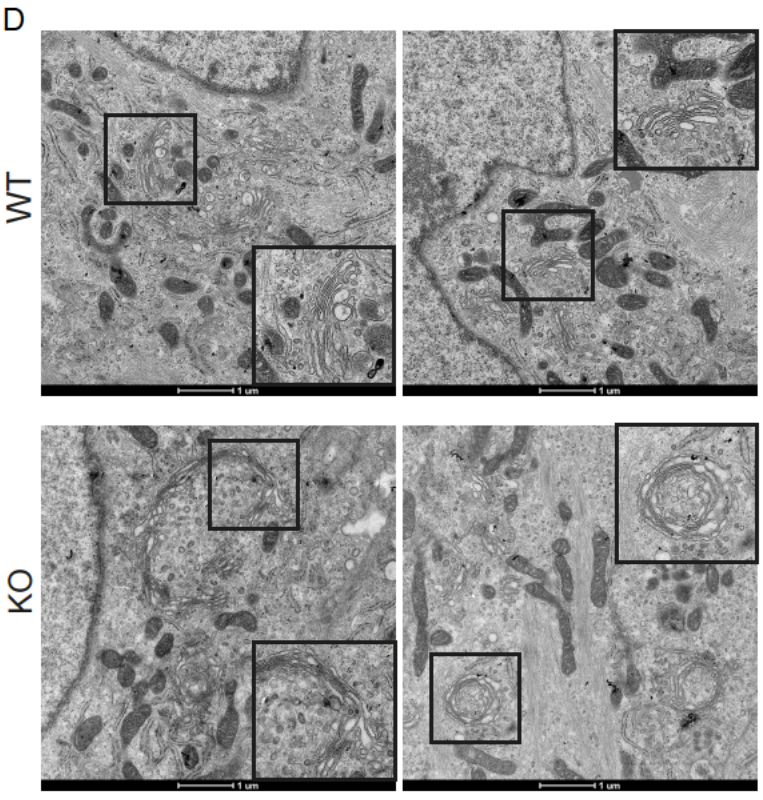

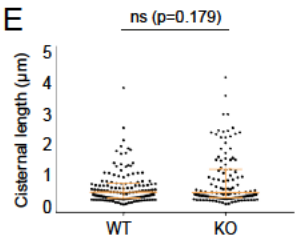

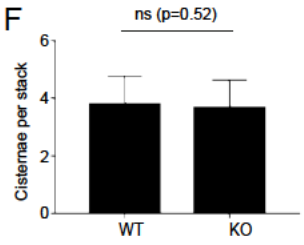

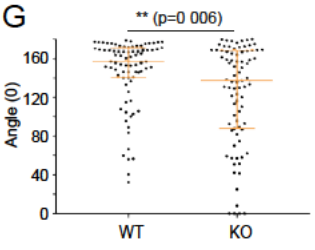

bioRxiv preprint doi: https://doi.org/10.1101/123547; this version posted April 3, 2017. The copyright holder for this preprint (which was not certified by peer review) is the author/funder, who has granted bioRxiv a license to display the preprint in perpetuity. It is made available under aCC-BY-NC-ND 4.0 International license.

Figure 4 – GALNT3 expression is lost in giantin KO cells. A-B. Western blots validating down-regulation of (A) GALNT3 and (B) CHST11 in KO cells. C. Maximum projection images of mixed populations of WT and KO cells immuno-labelled for giantin, GM130 and GALNT3. Arrows highlight giantin KO cells. D. Representative projections of WT and KO cells expressing FLAG-tagged GALNT3 fixed and stained as indicated. All scale bars 10μm.

bioRxiv preprint doi: https://doi.org/10.1101/123547; this version posted April 3, 2017. The copyright holder for this preprint (which was not certified by peer review) is the author/funder, who has granted bioRxiv a license to display the preprint in perpetuity. It is made available under a CC-BY-NC-ND 4.0 International license.

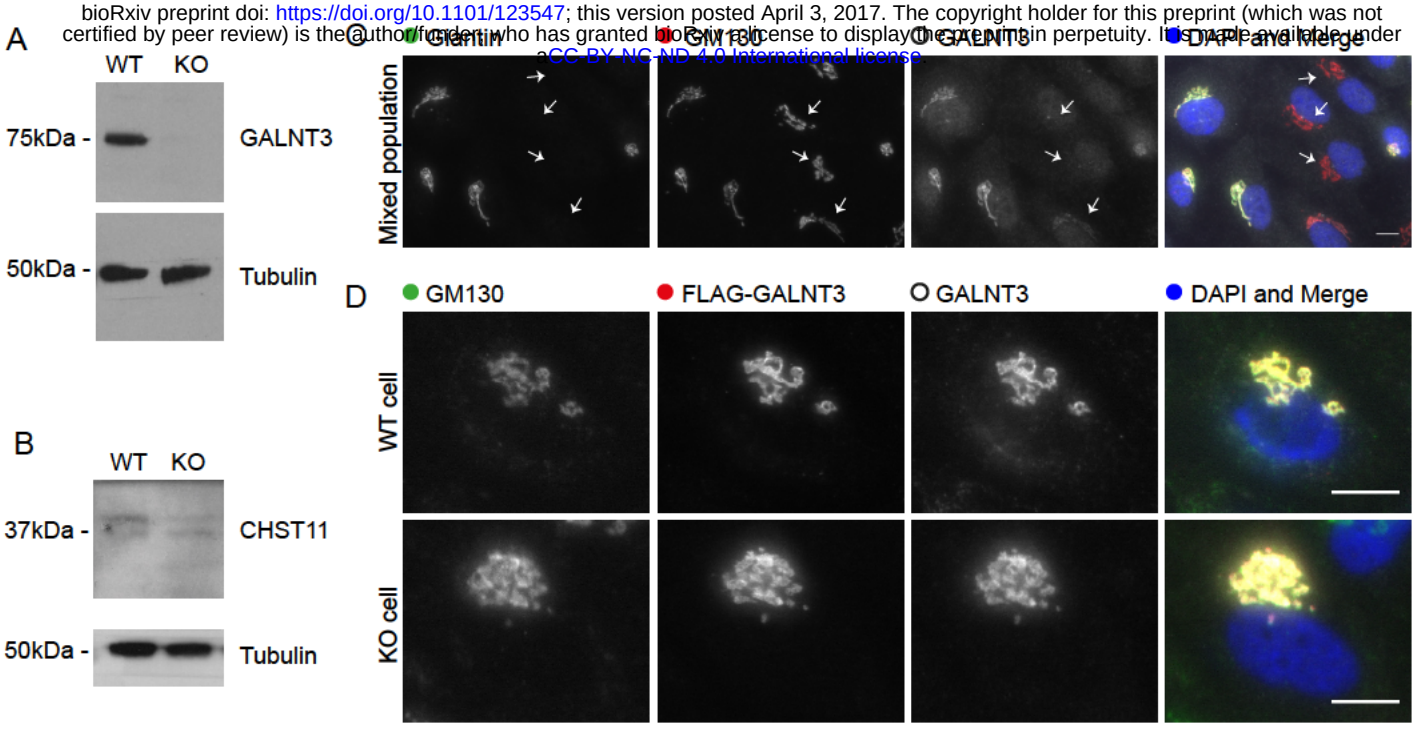

bioRxiv preprint doi: https://doi.org/10.1101/123547; this version posted April 3, 2017. The copyright holder for this preprint (which was not certified by peer review) is the author/funder, who has granted bioRxiv a license to display the preprint in perpetuity. It is made available under aCC-BY-NC-ND 4.0 International license.

Figure 5 – Giantin KO zebrafish have reduced *galnt3* expression and HFTC-like phenotypes. A. Real-time qPCR pairwise analysis of *galnt3* expression at 30dpf in two *golgb1* mutant zebrafish lines normalised to *gapdh* mRNA levels as housekeeping gene. Bars show mean expression for each mutant line relative to WT siblings (WT expression 1A.U depicted by dashed line). Each circle represents one individual (P value: *=<0.05, mean with standard deviation). B. microCT images and C. bone mass density measurements of the skulls of WT and *golgb1*$^{Q2948X/Q2948X}$. "E" marks position of the eyes, arrows depict area analysed. C. Data points show individual measurements (three per fish) of mean bone mass density (six points per measurement). P value: ** = < 0.01, mean and standard deviation. D. Ventral and E. lateral view representative microCT images showing craniofacial and spinal elements. Red arrows indicate the palatoquadrate (PQ) - Meckel's cartilage (MC) joint and green arrows ectopic deposits. (B-E) 3 females per group at 8 months post fertilisation. (A, C) Unpaired t-test was used as data were normally distributed. Scale bar 100µm.

bioRxiv preprint doi: https://doi.org/10.1101/123547; this version posted April 3, 2017. The copyright holder for this preprint (which was not certified by peer review) is the author/funder, who has granted bioRxiv a license to display the preprint in perpetuity. It is made available under aCC-BY-NC-ND 4.0 International license.

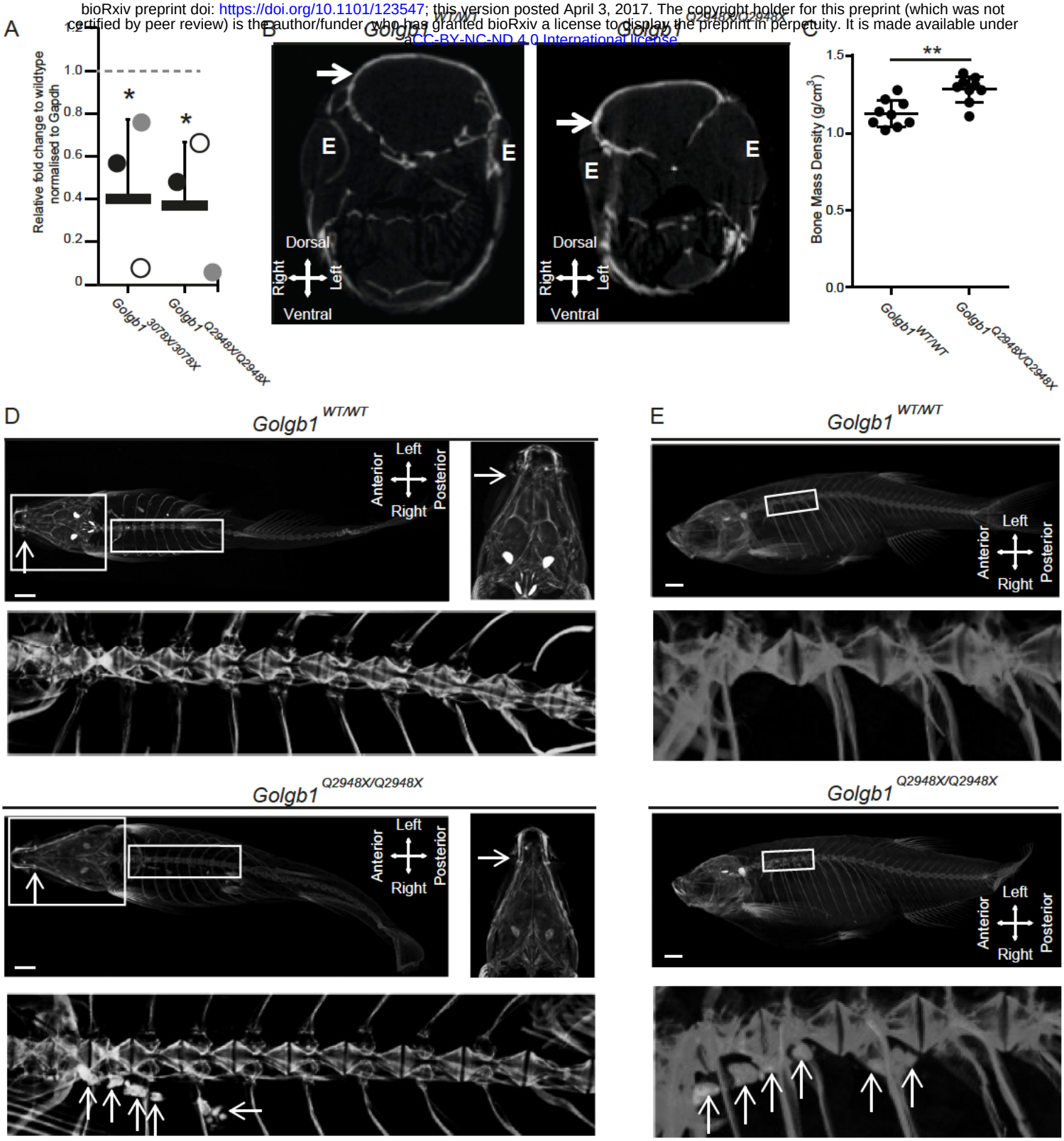

bioRxiv preprint doi: https://doi.org/10.1101/123547; this version posted April 3, 2017. The copyright holder for this preprint (which was not certified by peer review) is the author/funder, who has granted bioRxiv a license to display the preprint in perpetuity. It is made available under aCC-BY-NC-ND 4.0 International license.

Table 1: Glycosylation enzymes differentially expressed between WT and giantin KO RPE1 cells. Values shown are Fragments Per Kilobase of transcript per Million mapped reads (FPKM), the $\log_2$-fold change between these and the uncorrected p- and q-values (q being the false discovery rate (FDR)-adjusted p-value). All values were found significant (where p is greater than the FDR after Benjamini-Hochberg correction for multiple-testing). Pathway annotation and steady-state localisation was done manually based on gene ontology and published literature. Genes highlighted in red are downregulated and green are upregulated.

bioRxiv preprint doi: https://doi.org/10.1101/123547; this version posted April 3, 2017. The copyright holder for this preprint (which was not certified by peer review) is the author/funder, who has granted bioRxiv a license to display the preprint in perpetuity. It is made available under aCC-BY-NC-ND 4.0 International license.

Table 1

Gene	WT FPKM	KO FPKM	log2 (fold change)	p_value	q_value	Pathway	Organelle
GALNT5	0.0293487	0.693322	4.56216	5.00E-05	0.000214	N-Glycosylation	Golgi
ST6GALNAC3	0.302522	2.43643	3.00966	5.00E-05	0.000214	O-Glycosylation	Golgi
EXTL1	0.417023	1.00605	1.2705	5.00E-05	0.000214	N-Glycosylation	Golgi
CSPG5	0.351491	0.173152	-1.02145	0.0001	0.000408	O-Glycosylation	Golgi
GAL3ST3	0.252928	0.123266	-1.03695	0.00015	0.000591	Both N- and O-Glycosylation	Golgi
GALNT1	153.498	71.0283	-1.11175	5.00E-05	0.000214	O-Glycosylation	Golgi
DPY19L2P2	1.60655	0.718415	-1.16107	5.00E-05	0.000214	C-Glycosylation	Pseudogene
ST6GALNAC2	0.595085	0.24238	-1.29582	5.00E-05	0.000214	N-Glycosylation	Golgi
MGAT5B	6.70667	2.5532	-1.39329	5.00E-05	0.000214	N-Glycosylation	Golgi
GALNT16	9.52671	3.35166	-1.5071	5.00E-05	0.000214	O-Glycosylation	Golgi
B4GALNT4	9.7297	3.34711	-1.53948	5.00E-05	0.000214	O-Glycosylation	Golgi
B3GNT5	1.77188	0.581017	-1.60863	5.00E-05	0.000214	O-Glycosylation	Golgi
A4GALT	6.16651	1.7832	-1.78999	5.00E-05	0.000214	O-Glycosylation	Golgi
HS3ST1	1.92483	0.54196	-1.82847	5.00E-05	0.000214	O-Glycosylation	Golgi
LFNG	2.58988	0.653085	-1.98754	5.00E-05	0.000214	Both N- and O-Glycosylation	Golgi
CHST11	9.46678	1.97911	-2.25802	5.00E-05	0.000214	O-Glycosylation	Golgi
CHSY3	0.8767	0.161329	-2.44208	5.00E-05	0.000214	O-Glycosylation	Golgi
GALNT12	1.42884	0.199249	-2.84221	5.00E-05	0.000214	O-Glycosylation	Golgi
GBGT1	2.71611	0.233266	-3.54149	5.00E-05	0.000214	Glycolipid Glycosylation	Golgi
FUT4	0.904089	0.0770361	-3.55286	5.00E-05	0.000214	N-Glycosylation	Golgi
UGT8	4.82991	0.272601	-4.14714	5.00E-05	0.000214	Glycolipid Glycosylation	ER
GALNT3	8.35694	0.33148	-4.65598	5.00E-05	0.000214	O-Glycosylation	Golgi
ST6GAL2	0.699234	0.0208263	-5.0693	5.00E-05	0.000214	N-Glycosylation	Golgi
ST8SIA4	0.341234	0	-	5.00E-05	0.000214	N-Glycosylation	Golgi

bioRxiv preprint doi: https://doi.org/10.1101/123547; this version posted April 3, 2017. The copyright holder for this preprint (which was not certified by peer review) is the author/funder, who has granted bioRxiv a license to display the preprint in perpetuity. It is made available under a CC-BY-NC-ND 4.0 International license.

Legends to Supplemental information

Movie S1 relating to Figure 2 : RUSH trafficking in WT cells. WT cells transfected with Str-Kdel/ManI-SBP-EGFP were treated with biotin at T0 and imaged live as a single plane at 4 frames per minute.

Movie S2 relating to Figure 2: RUSH trafficking in KO cells. Giantin KO cells transfected with Str-Kdel/ManI-SBP-EGFP were treated with biotin at T0 and imaged live as a single plane at 4 frames per minute.

Movie S3 relating to Figure 5: *golgb1*$^{wt/wt}$ sibling fly through showing absence of ectopic deposits around the spine. 4 µm voxel size microCT scan.

Movie S4 relating to Figure 5: *golgb1*$^{Q2948X/Q2948X}$ mutant fly through showing ectopic deposits around the spine. 4 µm voxel size microCT scan.

Movie S5 relating to Figure 5: *golgb1*$^{wt/wt}$ sibling showing sagittal microCT slices through the spine. 21.8 µm voxel size.

Movie S6 relating to Figure 5: *golgb1*$^{Q2948X/Q2948X}$ mutant showing sagittal microCT slices with calcified deposits in the spine. 21.8µm voxel size.

Table S1 relating to Table 1: RNAseq results of pairwise comparison of wild-type and giantin KO cells. The first tab shows all data, the second shows those genes that have changed from than 2-fold, the third, those that have changed more than 3-fold.

Figure S1 relating to Figure 3: Brefeldin A treatment of KO cells. Representative maximum projection images of WT and KO cells treated with 5µm Brefeldin A for time indicated and immuno-labelled for cis-(GM130) and trans-(TGN46) Golgi markers. In wash out panels, cells were incubated in brefeldin A for 1 hour then washed 3x and left in growth media at 37oC for time indicated. Scale bars 10µm.

Figure S2 relating to Figure 4: Lectin labelling in giantin KO cells. Lectin labelling of WT and KO cells without permeabilization (A) and mixed populations of permeabilised WT and KO cells (B). Images are maximum projections. Scale bars 10µm. C. Western blots of WT and KO cell lysates probed with lectins. Arrows highlight missing bands.

Figure S3 relating to Figure 5: Ventral jaw element length ratios in 8 months old *golgb1*$^{Q2948X/Q2948X}$ zebrafish. A. Quantification of the relative distance from top of MC to the start of PQ and the width between the PQ-MC joint as displayed in (B) by the red and green line respectively. (A) Unpaired t-test (data were confirmed to be normally distributed; p value: *= <0.05, mean and standard deviation).

bioRxiv preprint doi: https://doi.org/10.1101/123547; this version posted April 3, 2017. The copyright holder for this preprint (which was not certified by peer review) is the author/funder, who has granted bioRxiv a license to display the preprint in perpetuity. It is made available under a CC-BY-NC-ND 4.0 International license.

Legend to Table S1: Excel spreadsheet of RNAseq data

Column number	Column name	Example	Description
1	Tested id	A1BG	A unique identifier describing the transcript, gene, primary transcript, or CDS being tested
2	gene	A1BG	The gene_name(s) or gene_id(s) being tested
3	locus	chr19:58346805--58362848	Genomic coordinates for easy browsing to the genes or transcripts being tested.
4	sample 1	RPE--WT	Label of the first sample
5	sample 2	RPE--giantin_KO	Label of the second sample
6	Test status	OK	Can be one of OK (test successful), NOTEST (not enough alignments for testing), LOWDATA (too complex or shallowly sequenced), HIDATA (too many fragments in locus), or FAIL, when an ill--conditioned covariance matrix or other numerical exception prevents testing.
7	FPKMx	1.78215	FPKM of the gene in sample x
8	FPKMy	2.77931	FPKM of the gene in sample y
10	Test stat	1.16871	The value of the test statistic used to compute significance of the observed change in FPKM
11	p	0.0513	The uncorrected p--value of the test statistic
12	q	0.10281	The FDR--adjusted p--value of the test statistic
13	significant	no	Can be either “yes” or “no”, depending on whether p is greater than the FDR after Benjamini-Hochberg correction for multiple--testing

bioRxiv preprint doi: https://doi.org/10.1101/123547; this version posted April 3, 2017. The copyright holder for this preprint (which was not certified by peer review) is the author/funder, who has granted bioRxiv a license to display the preprint in perpetuity. It is made available under aCC-BY-NC-ND 4.0 International license.

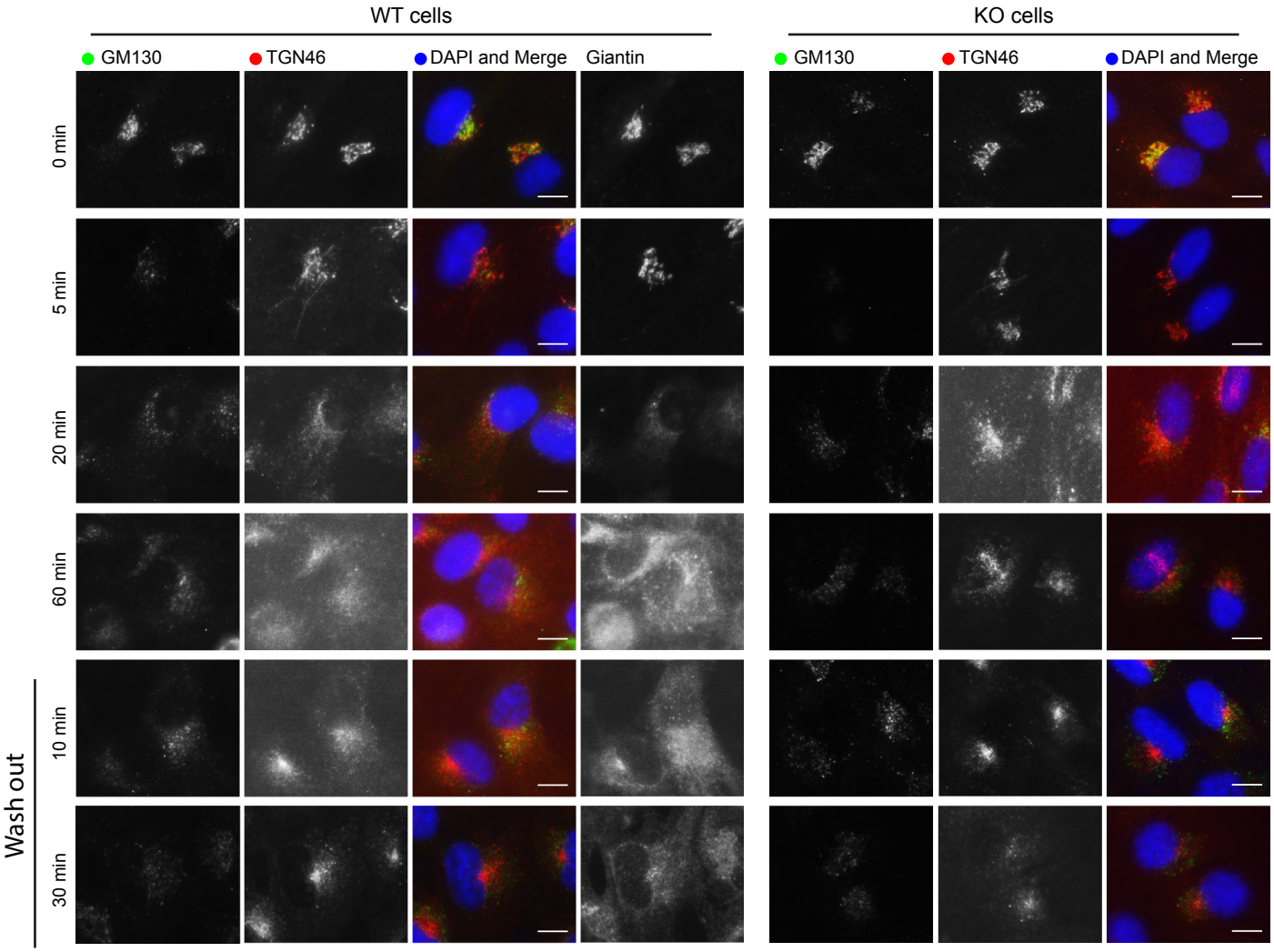

bioRxiv preprint doi: https://doi.org/10.1101/123547; this version posted April 3, 2017. The copyright holder for this preprint (which was not certified by peer review) is the author/funder, who has granted bioRxiv a license to display the preprint in perpetuity. It is made available under aCC-BY-NC-ND 4.0 International license.

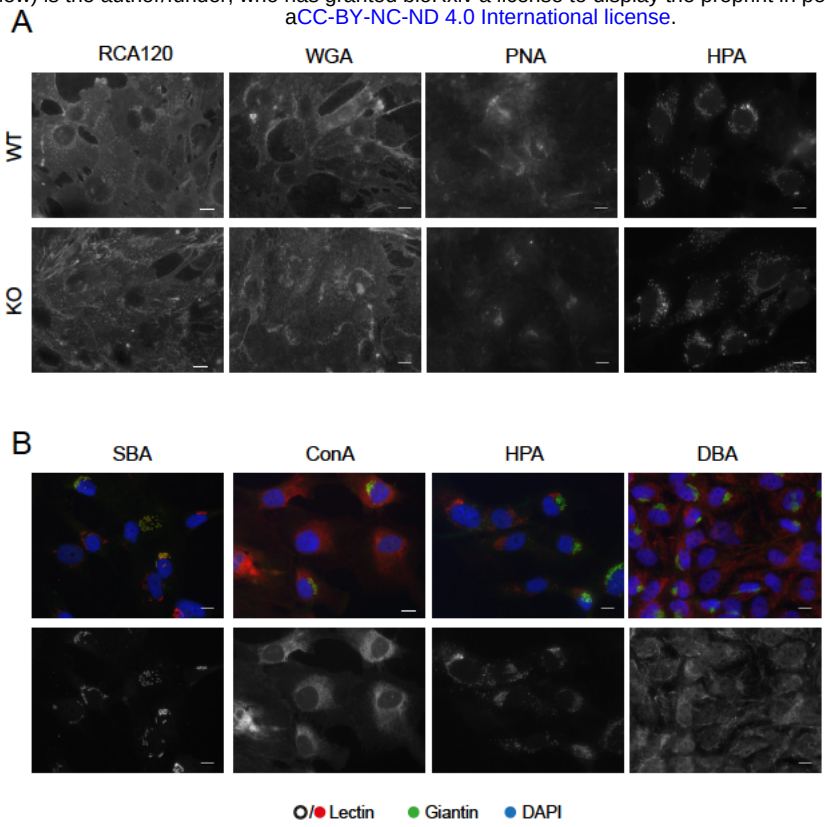

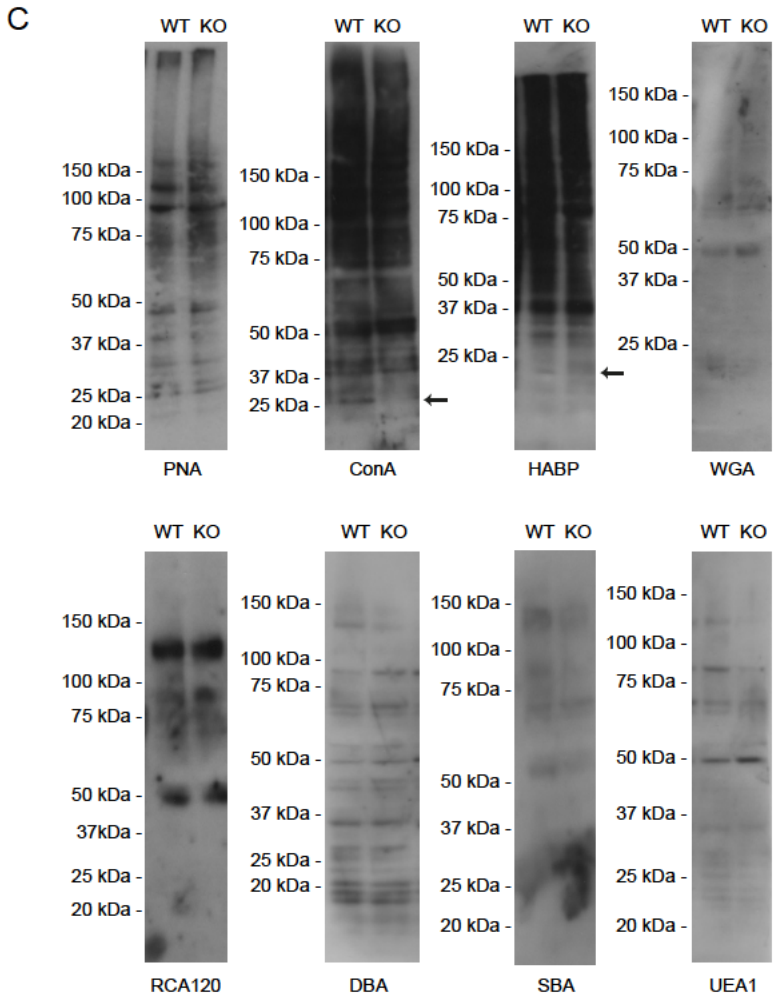

bioRxiv preprint doi: https://doi.org/10.1101/123547; this version posted April 3, 2017. The copyright holder for this preprint (which was not certified by peer review) is the author/funder, who has granted bioRxiv a license to display the preprint in perpetuity. It is made available under aCC-BY-NC-ND 4.0 International license.

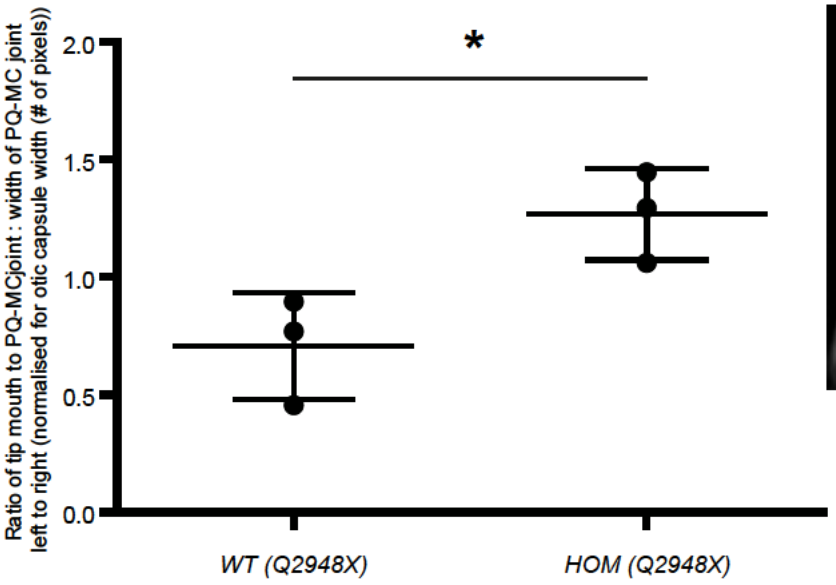

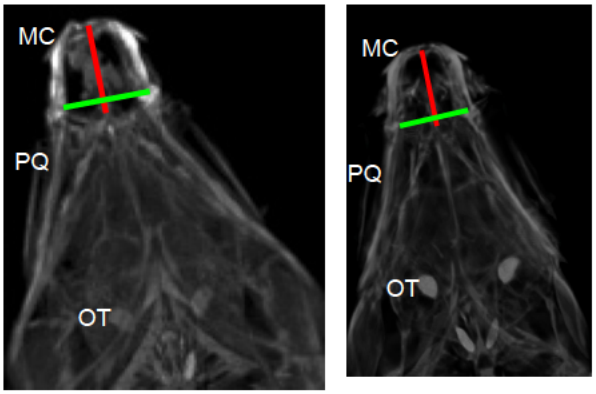

Tip mouth to PQ-MCjoint (red) and width of PQ-MC joint left to right (green)